10 Selected Applications Related to Control of Offshore Structures

Dynamic analyses of mechanical systems are often considered together with problems related to their control. With traditional ways of operating machines it the operator who decides what the working motions are. In contemporary machines, it is becoming commonplace to support the process of control. Control systems based on microprocessor technology (programmable drivers, onboard computers) are supposed to facilitate human work or even replace it. They enable realization of various strategies unachievable with manual control. Automated control is used also in offshore structures, including cranes. The criteria of control strategies may be different, for example:

- minimal duration of motion,
- minimal consumption of energy,
- accuracy of load positioning, including minimization of oscillations after the motion has ended,
- minimization of dynamic loads,
- stabilization of the load's position,
- minimization of the influence of sea waves on the device's dynamics.

The present chapter describes the basics of the method of selecting the drive functions based on dynamic optimization. Control of the drum of a winch of an A-frame type crane allowing it to compensate for vertical movements of the base due to sea waves is presented. For an offshore jib crane, an auxiliary system is proposed enabling the load to be positioned in three directions. In the last part, a concept of active compensation of waves for a drum's drive of a device for laying pipelines is discussed.

10.1 Dynamic Optimization

As former considerations imply, the equation of dynamics of a multibody system may be presented in the following:

$$\mathbf{A}\ddot{\mathbf{q}} = \mathbf{f}\left(t, \mathbf{q}, \dot{\mathbf{q}}, M\right), \tag{10.1}$$

$$\mathbf{q}(0) = \mathbf{q}_0, \tag{10.2.1}$$

$$\dot{\mathbf{q}}(0) = \mathbf{q}_1, \tag{10.2.2}$$

E. Wittbrodt et al.: Rigid Finite Element Method, OEO 1, pp. 203–244.
springerlink.com

where $\mathbf{q} = [q_1 \quad \cdots \quad q_n]^T$ – vector of generalized coordinates of the system,
$\mathbf{f}$ – excitation vector due to these forces: elasticity, damping, centrifugal, Coriolis, gyroscopic, and to the drives,
M – function giving the drive force or moment thereof, henceforth assumed to be a specified function of time,
$\mathbf{q}_0, \mathbf{q}_1$ – vectors of initial values of generalized coordinates and velocities.

The equations (10.1) are typically nonlinear and require numerical integration. Duration of their integration is closely related to the number n of generalized coordinates. Assuming large n considerably lengthens the calculations, whereas n being too small disables the mathematical model from adequately reflecting the dynamic properties of the system. The number n of generalized coordinates should therefore hit the balance between computation time and accuracy. Its choice depends largely on the purpose of the model.

In some cases, which are described in chapter 6, it is possible to write the equations (10.1) as a combined system of ordinary differential and nonlinear algebraic equations:

$$\mathbf{A}\,\ddot{\mathbf{q}} - \mathbf{D}\,\mathbf{R} = \mathbf{f}\left(t, \mathbf{q}, \dot{\mathbf{q}}, M\right), \tag{10.3.1}$$

$$\mathbf{\Lambda}\left(\mathbf{q}, \dot{\mathbf{q}}\right) = \mathbf{0}, \tag{10.3.2}$$

gdzie $\mathbf{A}, \mathbf{q}, \mathbf{f}$ – defined as in (10.1),
$\mathbf{R} = [R_1 \quad \cdots \quad R_m]^T$ – vector of constraint reactions,
$\mathbf{D} = \mathbf{D}(\mathbf{q})$ – matrix of coefficients,
$\mathbf{\Lambda} = [\lambda_1(\mathbf{q}, \dot{\mathbf{q}}) \quad \cdots \quad \lambda_m(\mathbf{q}, \dot{\mathbf{q}})]^T$ – vector of constraint equations,
m – number of components of the vector of constraint reactions.

To solve the equations (10.3) completed with initial conditions, a procedure is often applied whereby the constraint equations (10.3.2) are put in accelerative form by differentiation:

$$\mathbf{D}^T\ddot{\mathbf{q}} = \mathbf{W}\left(t, \mathbf{q}, \dot{\mathbf{q}}\right). \tag{10.4}$$

The equations (10.3.1) and (10.4) replace (10.3.2) and may be written as:

$$\begin{bmatrix} \mathbf{A} & -\mathbf{D} \\ \mathbf{D}^T & \mathbf{0} \end{bmatrix} \begin{bmatrix} \ddot{\mathbf{q}} \\ \mathbf{R} \end{bmatrix} = \begin{bmatrix} \mathbf{F}\left(t, \mathbf{q}, \dot{\mathbf{q}}, M\right) \\ \mathbf{W}\left(t, \mathbf{q}, \dot{\mathbf{q}}\right) \end{bmatrix}. \tag{10.5}$$

Further reasoning assumes that the equations of dynamics of the system take the form (10.1). For such equations, as just shown, can be easily extended to a system with constraints.

In the case of controlling working motions of machines, it is important to choose the drive function in such a way dependent on time that the intended goal

is achieved according to the set criteria. One method of finding appropriate drive functions is by optimization. The optimization task in this case is to choose the drive function $M(t)$ satisfying:

minimization of the functional:

$$\Omega\left(\mathbf{q}, \dot{\mathbf{q}}, M\right), \tag{10.6}$$

maintaining the boundary conditions:

$$e_i\left(\mathbf{q}, \dot{\mathbf{q}}\right) \leq 0 \qquad \text{for} \quad i = 1,..., n_e\,, \tag{10.7.1}$$

$$M_L(t) \leq M(t) \leq M_R(t)\,, \tag{10.7.2}$$

where n_e – number of boundary conditions,
$M_L(t), M_R(t)$ – known conditions constraining the drive function $M(t)$.

Note that it is necessary to know the vectors $\mathbf{q}, \dot{\mathbf{q}}$ corresponding to the function $M(t)$ in order to determine the functional Ω and the function e_i. This requires integration of the system's equations of motion (10.1) in each optimisation step. An optimization task formulated in this way is called a dynamic optimization task [Kręglewski T., et al., 1984], since its focus is the integration of equations of dynamics.

The problem of choosing the function $M(t)$ can be reduced to a classical optimization problem by discretisation. Let $t \in \langle 0, T \rangle$ and:

$$M_i = M(t_i) \qquad \text{for} \quad i = 1,..., p, \tag{10.8}$$

where p is defined in Fig. 10.1.

The value of $M(t)$ for $t \in \langle t_{i-1}, t_i \rangle$ may then be determined with cubic splines (Fig. 10.1), using the formula:

$$M^{(i)}(t) = a_i\left(t - t_{i-1}\right)^3 + b_i\left(t - t_{i-1}\right)^2 + c_i\left(t - t_{i-1}\right) + M_{i-1}\,, \tag{10.9}$$

whereby the coefficients a_i, b_i, c_i are chosen such that:

$$M^{(i)}(t_i) = M_i \qquad \text{for} \quad i = 1,..., p\,, \tag{10.10.1}$$

$$M^{(i)'}(t_i) = M^{(i+1)'}(t_i) \qquad \text{for} \quad i = 1,..., p-1\,, \tag{10.10.2}$$

$$M^{(i)''}(t_i) = M^{(i+1)''}(t_i) \qquad \text{for} \quad i = 1,..., p-1\,, \tag{10.10.3}$$

and:

$$M^{(0)'}(t_0) = 0 \qquad \text{or} \qquad M^{(0)''}(t_0) = 0\,, \tag{10.10.4}$$

$$M^{(p)'}(t_p) = 0 \qquad \text{or} \qquad M^{(p)''}(t_p) = 0\,. \tag{10.10.5}$$

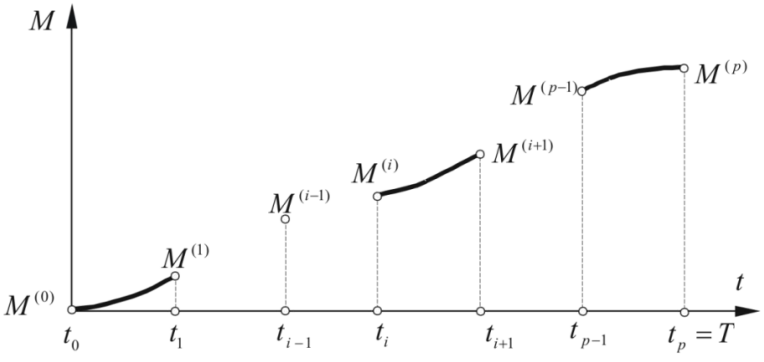

Fig. 10.1. Approximation of the function $M(t)$ with cubic splines

Equations (10.10) form a system of $3p$ linear algebraic equations with $3p$ unknowns $\left(a_1, b_1, c_1, ..., a_p, b_p, c_p\right)$. Its solution may be obtained easily by a recursive procedure.

If the drive function $M(t)$ is approximated by splines (10.9), then the optimization task consists in determining the p+1 values specified in (10.8). The decision variables in the considered task are therefore the components of the vector:

$$\mathbf{M} = \left[M_0 \quad \ldots \quad M_p\right]^T. \tag{10.11}$$

Eventually, the problems of defining the optimization tasks of drive functions, considered in further examples, reduce to finding values $M_0,\ldots,M_\mathrm{p}$ which constitute the coordinates of the vector of decision variables (10.11) minimizing the functional:

$$\Omega\left(\mathbf{q}, \dot{\mathbf{q}}, M_0, ..., M_p\right), \tag{10.12}$$

and also satisfying the conditions:

$$e_i\left(\mathbf{q}, \dot{\mathbf{q}}\right) \le 0 \qquad \text{for} \qquad i = 1,..., n_e, \tag{10.13.1}$$

$$M_{iL} \le M_i \le M_{iR}, \quad M_{iL} = M_L\left(t_i\right), \quad M_{iR} = M_R\left(t_i\right) \quad \text{for} \quad i = 1,..., p \tag{10.13.2}$$

The vectors $\mathbf{q}$ and $\dot{\mathbf{q}}$ are obtained by integrating the initial problem:

$$\mathbf{A}\,\ddot{\mathbf{q}} = \mathbf{f}\left(t, \mathbf{q}, \dot{\mathbf{q}}, M_0, ..., M_p\right), \tag{10.14.1}$$

$$\mathbf{q}\left(0\right) = \mathbf{q}_0, \quad \dot{\mathbf{q}}\left(0\right) = \mathbf{q}_1, \tag{10.14.2}$$

for $t \in \langle 0, T \rangle$.

Various methods may be used to solve this task. However, all of them are sensitive to the choice of the starting point, i.e. the initial values of $M_0,\ldots,M_\mathrm{p}$.

It can be easily noticed that the time cost of the optimization process directly depends on the time of integration of the equations of motion (10.14). Using for this case the mathematical models of the systems presented in preceding chapters would cause unacceptably long computations. It is the reason why the drive functions $M(t)$

are usually determined according to simplified models whose degrees of freedom are possibly few. This enables their possible application in real-time control. Verifying calculations which allow to assess the usefulness of the developed simplified models and control algorithms are carried out with respect to combined basic models, thus analogous to those described in earlier chapters.

10.2 Vertical Stabilization of Load of an A-Frame

In this chapter, two dynamic models of an A-frame are presented. In the first one, the flexibility of a frame is taken into account, while in the second this flexibility is omitted. In both cases the flexibility of rope is considered. The classical Rigid Finite Element Method has been used to discretise the frame – chapter 8.1. The algorithm of optimisation of the drive function for the drum of the hoisting winch is proposed. The goal of the optimisation is to ensure the stabilization of the load's position, i.e. to hold it at the required depth regardless of the ship's motion. In order to achieve appropriate numerical effectiveness, the optimisation problem has been solved using a simplified model of an A-frame.

10.2.1 A-Frame Model

The scheme of an A-frame and the most important points of it are presented in Fig. 10.2. The following denotations are used: F – supporting structure, P – pulley,

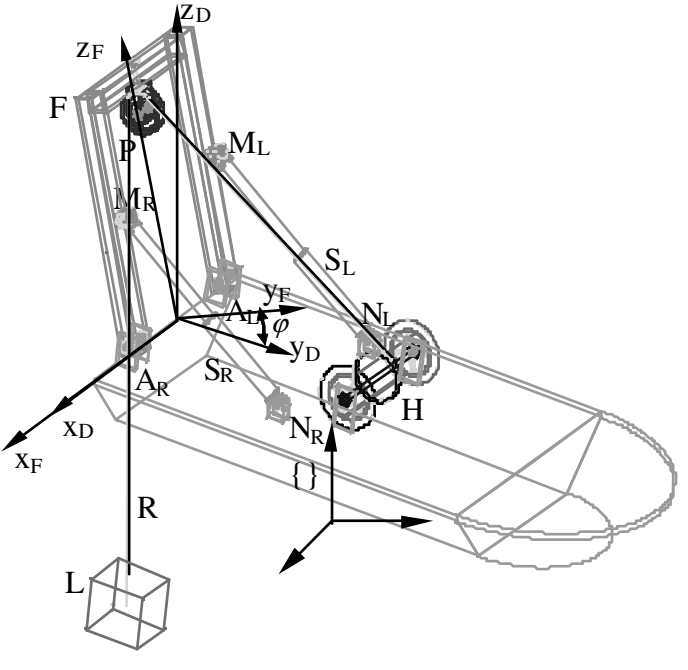

Fig. 10.2. A-frame scheme

R – rope, H – drum of the hoisting winch, L – load, S_R, S_L – right and left servomotor forces, N_R, N_L – connection points of servomotors to the A-frame, A_R, A_L – connection points of the A-frame to the deck, x_F, y_F, z_F and x_D, y_D, z_D – coordinate systems assigned to the supporting structure (frame) and to the deck, respectively.

The frame is the main element of the supporting structure in such cranes. In order to discretize the frame, the rigid finite element method can be applied.

In doctoral thesis [Fałat P., 2004], at first three beams were distinguished (right-1, top-2, left-3) in the frame. Then, each beam was divided into rigid finite elements and spring-damping elements (Fig. 10.3). This necessitates taking into account the reaction forces and moments at points B_L and B_B, and increases the number of constraint equations.

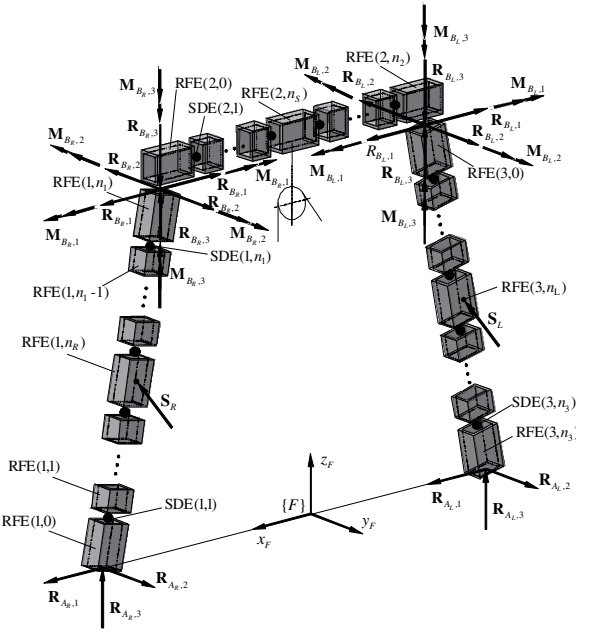

Fig. 10.3. A-frame divided into three beams which were divided into RFEs and SDEs

In this work we present a different approach. The frame is treated as one beam, which is divided into RFEs and SDEs. The obtained chain of rfes and sdes is presented in Fig. 10.4.

The position of each rfe of the undeformed beam is defined by the coordinate system ${}^{E}\{i\}$ with respect to the coordinate system $\{0\}$ of RFE 0, by a transformation matrix with constant components:

$$ {}^{0}_{E}\mathbf{T}_i = \begin{bmatrix} {}^{0}_{E}\mathbf{\Theta}_i & {}^{0}_{E}\mathbf{s}_i \\ \mathbf{0} & 1 \end{bmatrix}, \tag{10.15} $$

where ${}^{0}_{E}\mathbf{\Theta}_i$ is the matrix of cosines of the system ${}^{E}\{i\}$ with respect to $\{0\}$, and ${}^{0}_{E}\mathbf{s}_i$ is the vector of coordinates of the origin of the system ${}^{E}\{i\}$ in $\{0\}$ (Fig. 10.5).

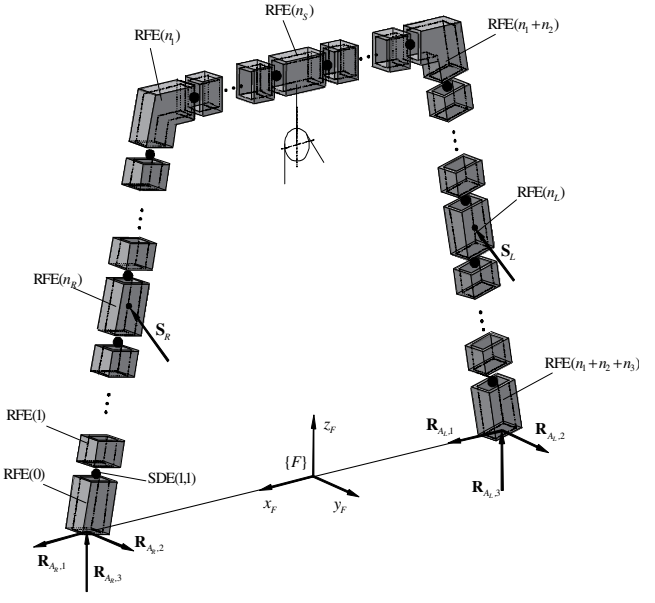

Fig. 10.4. A-frame as one beam, and its division into RFEs and SDEs

The coordinate system $\{i\}$ rigidly attached to RFE i moves together with the RFE when the beam is deformed. Its position in the coordinate system ${}^{E}\{i\}$ is defined by generalized coordinates of the i^{th} element, which are the components of the vector:

$$\mathbf{q}_i = \begin{bmatrix} \mathbf{r}_i \\ \boldsymbol{\varphi}_i \end{bmatrix}, \tag{10.16}$$

where $\mathbf{r}_i = \begin{bmatrix} x_i & y_i & z_i \end{bmatrix}^T$ and $\boldsymbol{\varphi}_i = \begin{bmatrix} \varphi_i & \theta_i & \psi_i \end{bmatrix}^T$ are vectors of displacements and rotation angles presented in Fig. 10.5.

If we assume that angles $\varphi_i, \theta_i, \psi_i$ are small, then the transformation matrix from the local coordinate system $\{i\}$ to the system ${}^{E}\{i\}$ takes the following form:

$$\mathbf{T}_i = \begin{bmatrix} 1 & -\psi_i & \theta_i & x_i \\ \psi_i & 1 & -\varphi_i & y_i \\ -\theta_i & \varphi_i & 1 & z_i \\ 0 & 0 & 0 & 1 \end{bmatrix} = \mathbf{I} + \sum \mathbf{D}_j q_{i,j}\,, \tag{10.17}$$

where $\mathbf{q}_i = \begin{bmatrix} x_i & y_i & z_i & \varphi_i & \theta_i & \psi_i \end{bmatrix}^T$,

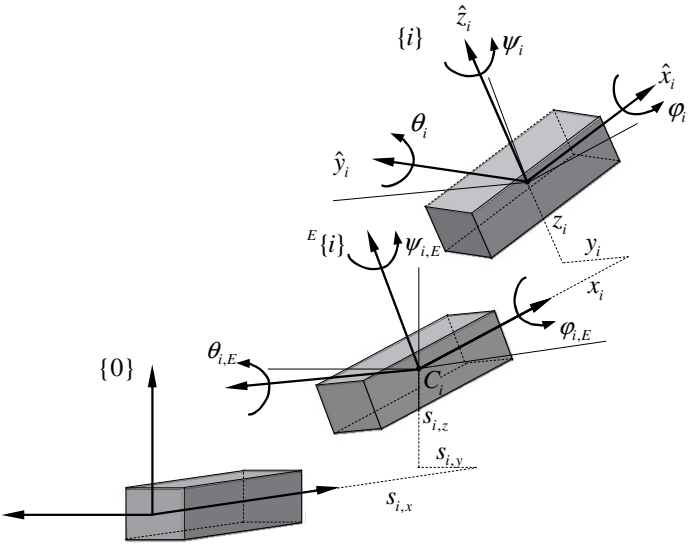

Fig. 10.5. The systems of i^{th} RFE and generalized coordinates

$$\mathbf{D}_1 = \begin{bmatrix} 0 & 0 & 0 & 1 \\ 0 & 0 & 0 & 0 \\ 0 & 0 & 0 & 0 \\ 0 & 0 & 0 & 0 \end{bmatrix}, \quad \mathbf{D}_2 = \begin{bmatrix} 0 & 0 & 0 & 0 \\ 0 & 0 & 0 & 1 \\ 0 & 0 & 0 & 0 \\ 0 & 0 & 0 & 0 \end{bmatrix}, \quad \mathbf{D}_3 = \begin{bmatrix} 0 & 0 & 0 & 0 \\ 0 & 0 & 0 & 0 \\ 0 & 0 & 0 & 1 \\ 0 & 0 & 0 & 0 \end{bmatrix},$$

$$\mathbf{D}_4 = \begin{bmatrix} 0 & 0 & 0 & 0 \\ 0 & 0 & -1 & 0 \\ 0 & 1 & 0 & 0 \\ 0 & 0 & 0 & 0 \end{bmatrix}, \quad \mathbf{D}_5 = \begin{bmatrix} 0 & 0 & 1 & 0 \\ 0 & 0 & 0 & 0 \\ -1 & 0 & 0 & 0 \\ 0 & 0 & 0 & 0 \end{bmatrix}, \quad \mathbf{D}_6 = \begin{bmatrix} 0 & -1 & 0 & 0 \\ 1 & 0 & 0 & 0 \\ 0 & 0 & 0 & 0 \\ 0 & 0 & 0 & 0 \end{bmatrix}.$$

The transformation matrix $\mathbf{B}_i$ that allows us to transform coordinates from the local coordinate system $\{i\}$ to the inertial coordinate system $\{\}$ according to the relation:

$$\mathbf{r} = \mathbf{B}_i \, \mathbf{r}_i , \tag{10.18}$$

where $\mathbf{r}_i$ – vector of coordinates in local system $\{i\}$,

$\mathbf{r}$ – vector of coordinates in base system $\{\}$,

has the form:

$$\mathbf{B}_i = \mathbf{B}_i(t, \mathbf{q}_i) = \mathbf{T}_D \; \mathbf{T}_F \; {}^0_E\mathbf{T}_i \; \mathbf{T}_i = \mathbf{A}(t) \; \mathbf{P}_i(\mathbf{q}_i) , \tag{10.19}$$

where $\mathbf{T}_D = \mathbf{T}_D(t)$ – defines the motion of the ship deck with respect to the base system $\{\}$,

$\mathbf{T}_F = \mathbf{T}_F(\varphi(t))$ – describes the rotation of the frame in the coordinate system of the deck $\{D\}$,

${}^0_E\mathbf{T}_i = \text{const}$ – defined in (10.15),

$\mathbf{T}_i = \mathbf{T}_i(\mathbf{q}_i)$ – presented in (10.17),

$\mathbf{A}(t) = \mathbf{T}_D\,\mathbf{T}_F$,

$\mathbf{P}_i = {}^0_E\mathbf{T}_i\,\mathbf{T}_i$.

In the case when the axes of the local coordinate system $\{i\}$ are chosen as principal central axes of the RFE, the mass and inertial features of the RFE *i* are defined by: its mass, m_i, and $J_{i,j}$ $(j = 1, 2, 3)$ which are mass moments of inertia with respect to the axis $\hat{x}_i$, $\hat{y}_i$, $\hat{z}_i$.

The equations of motion of the system considered can be obtained from Lagrange equations. This approach requires the kinetic and potential energy of the system to be defined. The kinetic energy of the RFE *i* can be calculated as:

$$E_i = \frac{1}{2}\text{tr}\{\dot{\mathbf{B}}_i\,\mathbf{H}_i\,\dot{\mathbf{B}}_i^T\}, \tag{10.20}$$

where $\mathbf{H}_i$ – the pseudo-inertia matrix defined as in (5.11).

Following the considerations, we can obtain:

$$\frac{d}{dt}\frac{\partial E_i}{\partial \dot{\mathbf{q}}_i} - \frac{\partial E_i}{\partial \mathbf{q}_i} = \mathbf{M}_i\ddot{\mathbf{q}}_i + \mathbf{e}_i, \tag{10.21}$$

where $\mathbf{M}_i = diag\left[m_i, m_i, m_i, J_z, J_y, J_x\right]$,

$e_{i,j} = e_{i,j}(t, \mathbf{q}_i, \dot{\mathbf{q}}_i) = \text{tr}\left\{\mathbf{B}_{i,j}\mathbf{H}_i\left[\ddot{\mathbf{A}}\mathbf{P}_i + 2\dot{\mathbf{A}}\dot{\mathbf{P}}_i\right]^T\right\}$,

$\mathbf{B}_{i,j} = \mathbf{A}\dfrac{\partial \mathbf{P}_i}{\partial q_{i,j}}$,

$\dfrac{\partial \mathbf{P}_i}{\partial q_{i,j}} = {}^0_E\mathbf{T}_i\mathbf{D}_j = \text{const}$.

The kinetic energy of the frame can be expressed by:

$$E = \sum_{i=0}^{n} E_i, \tag{10.22}$$

where $n = n_1 + n_2 + n_3 + 1$,

and it is possible to calculate:

$$\frac{d}{dt}\frac{\partial E}{\partial \dot{\mathbf{q}}_F} - \frac{\partial E}{\partial \mathbf{q}_F} = \mathbf{M}_F \ddot{\mathbf{q}}_F + \mathbf{e}_F , \tag{10.23}$$

where $\mathbf{M}_F = \text{diag}\left[\mathbf{M}_0, \ldots, \mathbf{M}_n\right]$,

$\mathbf{e}_F = \left[\mathbf{e}_0^T \ldots \mathbf{e}_n^T\right]^T$,

$\mathbf{q}_F = \left[\mathbf{q}_0^T \ldots \mathbf{q}_n^T\right]^T$.

The potential energy of deformation of SDEs can be expressed as follows:

$$V_F = \frac{1}{2}\mathbf{q}_F^T \mathbf{K}_F \mathbf{q}_F , \tag{10.24}$$

where $\mathbf{K}_F$ – the stiffness matrix with constant coefficients.

Similarly, one can calculate the dissipation of energy as:

$$D_F = \frac{1}{2}\dot{\mathbf{q}}_F^T \mathbf{L}_F \dot{\mathbf{q}}_F , \tag{10.25}$$

where $\mathbf{L}_F$ – the damping matrix with constant elements.

From what has been written above, one can calculate:

$$\frac{\partial V_F}{\partial \mathbf{q}_F} = \mathbf{K}_F \mathbf{q}_F , \tag{10.26.1}$$

$$\frac{\partial D_F}{\partial \dot{\mathbf{q}}_F} = \mathbf{L}_F \dot{\mathbf{q}}_F . \tag{10.26.2}$$

The potential energy of gravity forces of the frame can be calculated as:

$$V_g^F = \sum_{i=0}^{n} m_i g\, \boldsymbol{\theta}_3 \mathbf{B}_i \mathbf{r}_{C,i} , \tag{10.27}$$

where $\mathbf{r}_{C,i} = [0 \quad 0 \quad 0 \quad 1]$.

So:

$$\frac{\partial V_g^F}{\partial \mathbf{q}_F} = \mathbf{G}_F , \tag{10.28}$$

where $\mathbf{G}_F = \left[\mathbf{G}_0^T, \ldots, \mathbf{G}_n^T\right]^T$,

$\mathbf{G}_i = \left[G_{i,1}, \ldots, \mathbf{G}_{i,6}\right]^T$,

$G_{i,j} = m_i\, g\, \boldsymbol{\theta}_3 \mathbf{D}_j \mathbf{r}_{C,i}$,

$\mathbf{D}_j$ – defined in (10.17).

Energy of Load and Drum of the Hoisting Winch

The load is modelled as a particle. The vector of its generalized coordinates is expressed in the following form $\mathbf{q}_L = \begin{bmatrix} x_L & y_L & z_L \end{bmatrix}^T$. The angle of rotation of the drum of the hoisting winch is denoted as φ_H. Kinetic energy of the load and the drum can then be calculated as:

$$T_R = \frac{1}{2} m_L \, \dot{r}_L^2 + \frac{1}{2} I_H \, \dot{\varphi}_H^2 , \tag{10.29}$$

where I_H – moment of inertia mass of the drum,
$\dot{r}_L^2 = \dot{x}_L^2 + \dot{y}_L^2 + \dot{z}_L^2$.

Potential energy of the load is determined as:

$$V_g^L = m_L \, g \, z_L . \tag{10.30}$$

Elastic Deformation of the Rope

The rope system of the A-frame is presented in the Fig. 10.6. It is assumed that the radii of pulleys are small compared to the dimensions of the whole mechanism, and also that the rope passes through points S and H – centres of the pulley and the drum, respectively. Because the radii of pulleys are small and the length of the rope may be hundreds of meters, this simplification can be seen as admissible.

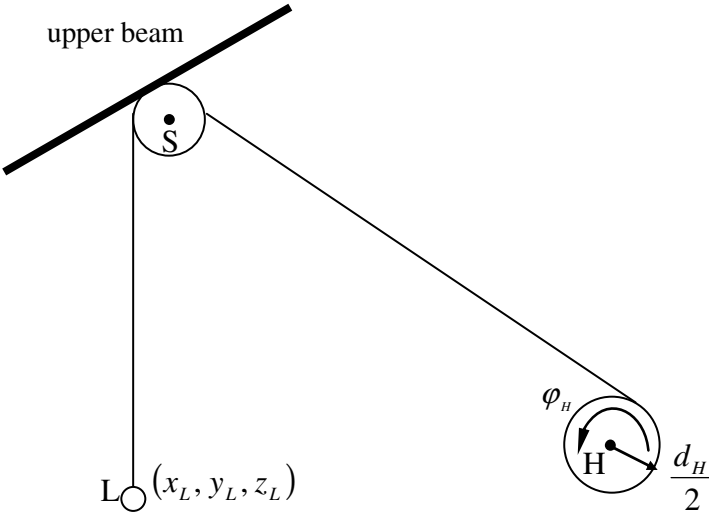

Fig. 10.6. Rope system of the A-frame

Potential energy of elastic deformation of the rope and its dissipation can be expressed in the following forms:

$$V_R = \frac{1}{2} c_R \delta_R \Delta_R^2 , \tag{10.31}$$

$$D_R = \frac{1}{2} d_R \delta_R \dot{\Delta}_R^2 , \tag{10.32}$$

where $\delta_R = \begin{cases} 0 & \text{if} \quad \Delta_R \le 0 \\ 1 & \text{if} \quad \Delta_R > 0 \end{cases}$,

$\Delta_R = |LS| + |SH| - l_0 - \varphi_H \frac{d_H}{2}$,

$|LS| = |\mathbf{r}_L - \mathbf{r}_S|$,

$|SH| = |\mathbf{r}_s - \mathbf{r}_H|$,

$c_R = \frac{E_R F_R}{l}$ – stiffness coefficient of the rope,

d_R – damping coefficient of the rope,

l_0, l – initial and current length of the rope, respectively,

E_R – Young's modulus of the rope material,

F_R – cross-section of the rope,

d_H – diameter of the drum.

Motion Equations

The vector of A-frame generalised coordinates can be presented in the form:

$$\mathbf{q} = \begin{bmatrix} \mathbf{q}_F \\ \mathbf{q}_R \end{bmatrix}, \tag{10.33}$$

where $\mathbf{q}_F$ – the vector of generalised coordinates of the discretised frame defined in (10.23) and vector $\mathbf{q}_R = [x_L \quad y_L \quad z_L \quad \varphi_H]^T$ contains generalised coordinates of the load and the angle of rotation of the drum.

Then, the equations of motion of the system can be written as:

$$\mathbf{M}\ddot{\mathbf{q}} + \mathbf{L}\dot{\mathbf{q}} + \mathbf{K}\mathbf{q} = \mathbf{Q} + \mathbf{D}\mathbf{R} , \tag{10.34}$$

where $\mathbf{M} = \begin{bmatrix} \mathbf{M}_F & 0 \\ 0 & \mathbf{M}_L \end{bmatrix}$,

$\mathbf{M}_L = diag\,[m_L, m_L, m_L, I_H]$,

$\mathbf{L} = \begin{bmatrix} \mathbf{L}_F & 0 \\ 0 & 0 \end{bmatrix}$, $\mathbf{K} = \begin{bmatrix} \mathbf{K}_F & 0 \\ 0 & 0 \end{bmatrix}$,

$$\mathbf{Q} = \begin{bmatrix} -\dfrac{\partial V_g^F}{\partial \mathbf{q}_F} - \dfrac{\partial V_R}{\partial \mathbf{q}_F} - \dfrac{\partial D_R}{\partial \dot{\mathbf{q}}_F} - \mathbf{e}_F \\ -\dfrac{\partial V_g^L}{\partial \mathbf{q}_R} - \dfrac{\partial V_R}{\partial \mathbf{q}_R} - \dfrac{\partial D_R}{\partial \dot{\mathbf{q}}_R} - \mathbf{e}_L \end{bmatrix},$$

D, **R** – matrix and vector of reaction forces,

$\dfrac{\partial V_R}{\partial \mathbf{q}_F}, \dfrac{\partial V_R}{\partial \mathbf{q}_R}, \dfrac{\partial D_R}{\partial \dot{\mathbf{q}}_F}, \dfrac{\partial D_R}{\partial \dot{\mathbf{q}}_R}$ can be calculated as in chapter 9.1.1 and involves nonlinear terms.

Forces of reactions on the frame are presented in Fig. 10.4. Vector **R** of generalised forces then specifically includes:

- reaction $\mathbf{R}_{AL} = \begin{bmatrix} R_{AL,x} & R_{AL,y} & R_{AL,z} \end{bmatrix}^T$,
- reaction $\mathbf{R}_{AR} = \begin{bmatrix} R_{AR,x} & R_{AR,y} & R_{AR,z} \end{bmatrix}^T$,
- and forces in servomotors S_L and S_R.

These forces can be written in the vector form:

$$\mathbf{R} = \begin{bmatrix} S_R & S_L & \mathbf{R}_{AR}{}^T & \mathbf{R}_{AL}{}^T \end{bmatrix}^T . \tag{10.35}$$

Finally, the mathematical model of an A-frame has been written in the form of a system of differential equations of the second order (10.34) and constraint equations in acceleration form:

$$\mathbf{D}^T \ddot{\mathbf{q}} = \mathbf{W} , \tag{10.36}$$

where $\mathbf{W} = \mathbf{W}(\mathbf{q}, \dot{\mathbf{q}})$.

In these equations, there are: $n_q = 6(1+n)+4$ (components of vector **q**) plus $n_R = 2 + 2 \cdot 3 = 8$ (components of vector **R**) unknowns. So, the number of unknowns is equal to the sum of numbers of equations (10.34) and (10.36).

10.2.2 Optimisation Problem

One of the major problems connected with the design and control of cranes is the choice of the drive functions which ensure proper motion of the system**.** In the case of A-frame, a very important problem is the stabilisation of load position, regardless of motion of the ship caused by sea waves. Using the drive of the drum of the hoisting winch we can try to solve this problem. Time courses of drive

functions can be defined in the optimisation process. In the book, the objective function is assumed to be in one of the following forms:

$$\Omega_1 = \int_0^{t_k} \left[z_L - h \right]^2 \rightarrow \min , \tag{10.37.1}$$

$$\Omega_2 = \max_{0 \le t \le t_k} \left| z_L - h \right| \rightarrow \min , \tag{10.37.2}$$

where z_L – load coordinate,
h – required depth.

This means that one expects that as the result of optimisation the course of the function $\varphi_H(t)$ will be obtained which minimizes the average or maximal value of deviation of load position from the required amount. During the optimisation process, the parameters of ship hull movement and coordinates of the winch position have been assumed to be known.

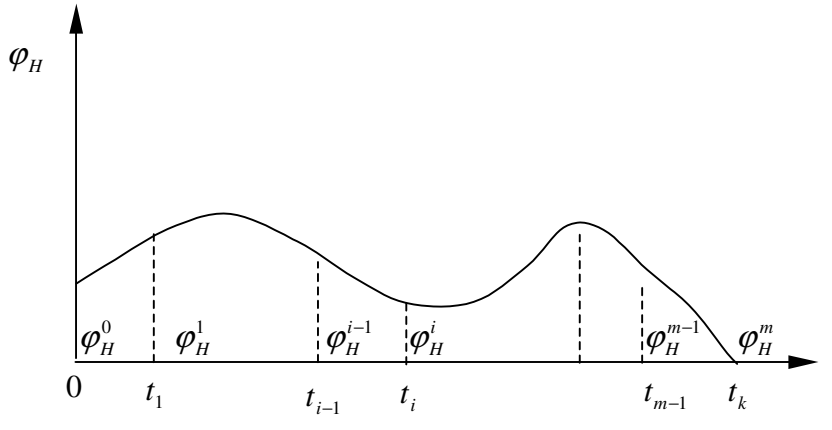

Fig. 10.7. The decisive variables

In this chapter, we assume that the function φ_H which describes the function $\varphi_H(t)$ defining the rotation angle of the winch drum has either the form:

$$\varphi_H(t) = a_i t^3 + b_i t^2 + c_i t + d_i , \text{ for } t \in < t_{i-1}, t_i > , \tag{10.38.1}$$

where $i = 1, \ldots, m$,
a_i, b_i, c_i, d_i – coefficients taken as shown in chapter 10.1 for spline functions of the third order,
t_i – point in interval $< 0, t_k >$ (Fig. 10.7),

or that introduced by [Maczyński A., 2005]:

$$\varphi_H(t) = A_0 + \sum_{i-=1}^{s} A_i \sin\left(\omega_i t + \alpha_{i,0}\right) \quad \text{for} \quad t \in \langle t_{i-1}, t_i \rangle, \tag{10.38.2}$$

where A_i – amplitudes,
ω_i – frequencies,
$\alpha_{i,0}$ – phase angles.

As the decisive variables in the optimisation task we can choose:

$$\mathbf{X} = \left[\varphi_H^0, \varphi_H^1, \ldots, \varphi_H^m\right]^T \tag{10.39.1}$$

in the case (10.38.1), i.e. when spline functions are applied (Fig. 10.7), or:

$$X = \left[A_0, A_1, \omega_1, \alpha_{1,0}, \ldots A_s, \omega_s, \alpha_{s,0}\right]^T \tag{10.39.2}$$

in the case when a pseudo-harmonic response is assumed.

In either case, at every step of the optimisation, the equations of motion of the system have to be integrated for $t \in \langle 0, t_k \rangle$ in order to calculate the value of the functional $\Omega_{1,2}$ from (10.37). Such an approach requires high numerical efficiency in solving A-frame equations of motion. For that reason, the optimisation problem has been solved for the simplified model of an A-frame.

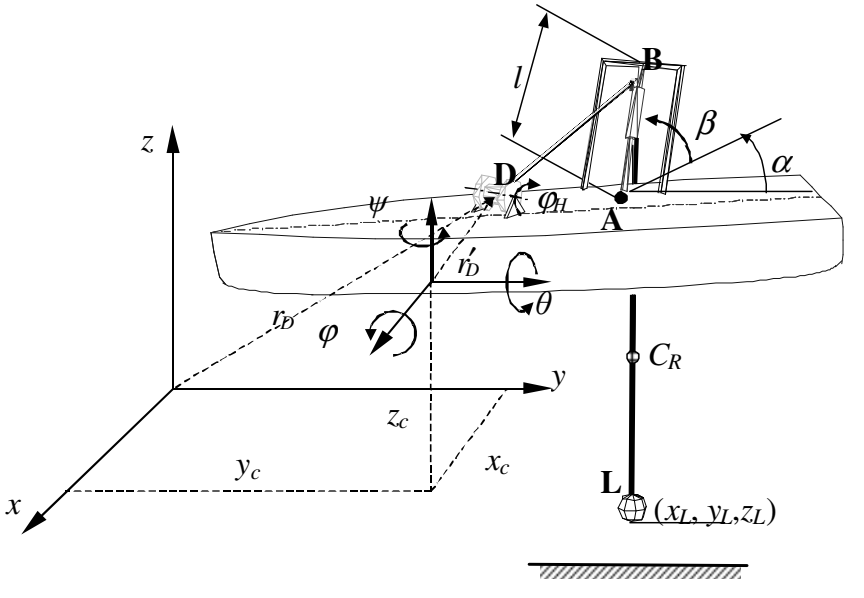

Fig. 10.8. Scheme of the simplified model

In the simplified model of an A-frame, ideal stiffness of the frame has been assumed (Fig. 10.8). However, flexibility of the rope has been taken into consideration. The water damping ratio has not been taken into account. Ship motion has been assumed to be determined, by known functions:

$$\begin{aligned} x_c &= x_c(t) \\ y_c &= y_c(t) \\ z_c &= z_c(t) \\ \varphi &= \varphi(t) \\ \theta &= \theta(t) \\ \psi &= \psi(t) \end{aligned} . \tag{10.40}$$

This means that matrix $\mathbf{T}_D$, from (10.19), has the form:

$$\mathbf{T}_D = \begin{bmatrix} c\psi c\theta & c\psi s\theta s\varphi - s\psi c\varphi & c\psi s\theta c\varphi + s\psi s\varphi & x_c \\ s\psi c\theta & s\psi s\theta s\varphi + c\psi c\varphi & s\psi s\theta c\varphi - c\psi s\varphi & y_c \\ -s\theta & c\theta s\varphi & c\theta c\varphi & z_c \\ 0 & 0 & 0 & 1 \end{bmatrix}, \tag{10.41}$$

where $c()=\cos()$ and $s()=\sin()$.

The frame angles are assumed to be constant.

Kinetic and potential energy of the system can be expressed in the form:

$$T = \frac{1}{2} m_L \left(\dot{x}_L^2 + \dot{y}_L^2 + \dot{z}_L^2 \right), \tag{10.42.1}$$

$$V = \frac{1}{2} \delta_R \, c_R \, \Delta_R^2 + m_L \, g \, z_L , \tag{10.42.2}$$

$$D = \frac{1}{2} \delta_R \, d_R \, \dot{\Delta}_R , \tag{10.42.3}$$

where m_L, δ_R, c_R, d_R – defined in (10.31),

$\Delta_R = |DB| + |BN| - l_0 + \varphi_H \, r_H$.

Lagrange's equations of the second order have been used to determine the equations of motion of the system. The details are presented in [Fałat P., et al., 2005]. These differential equations of the second order have been integrated using the Runge-Kutta method. The Nelder-Meads method has been applied in order to solve the optimisation task.

10.2.3 Numerical Simulations

It should be mentioned that the numerical model of the A-frame presented in chaper 10.2.2 has been used in the Norwegian company TTS-Aktro from Molde for a fast analysis of forces and stresses at the initial stage of choosing parameters of the system and for cost calculations. In order to verify the model, the results obtained using our program (RFEM) have been compared with those obtained using commercial FEM program (NASTRAN package) [Fałat P., et al., 2001]. There have been compared reactions in joints, stresses and deflections of beams obtained. Some examples are presented in Fig. 10.9.

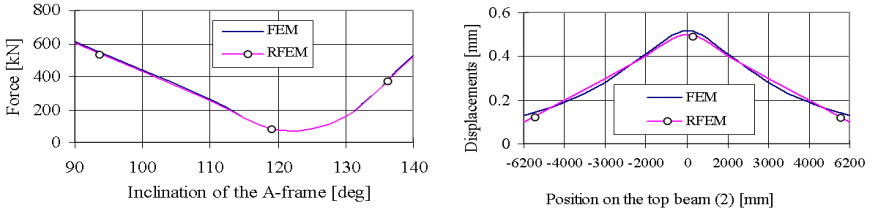

Fig. 10.9. Comparison of FEM and RFEM models

A comparison of the results obtained using RFEM model with those from Ansys-Adams systems in dynamical conditions can be find in [Fałat P., 2004] and same of them are presented Fig. 10.10.

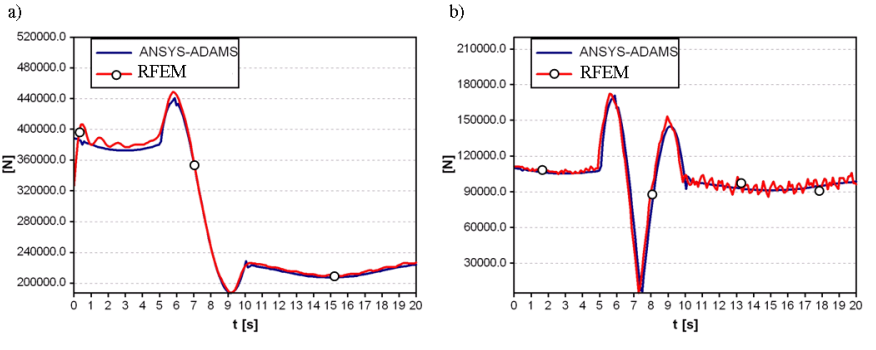

Fig. 10.10. Comparison of RFEM and Ansys-Adams models: a) vertical reaction in the A-frame leg, b) force in the servo-motor

Numerical simulations related to the load stabilisation problem have been carried out for the rectangular A-frame with lifting capacity up to 100 Mg. The

main geometrical parameters of the crane are presented in Fig 10.11. The value of load coordinates z_L, for which the optimisation process has been carried out is h=-300 m, mass of load m_L=100 Mg, and the motion of the ship is defined as:

$$\begin{aligned} x_c(t) &= 1\sin\left(\frac{2\pi}{6}t\right) \\ y_c(t) &= 0 \\ z_c(t) &= 2\sin\left(\frac{2\pi}{12}t\right). \\ \varphi &= 0 \\ \theta &= 0 \\ \psi &= 0 \end{aligned} \tag{10.43}$$

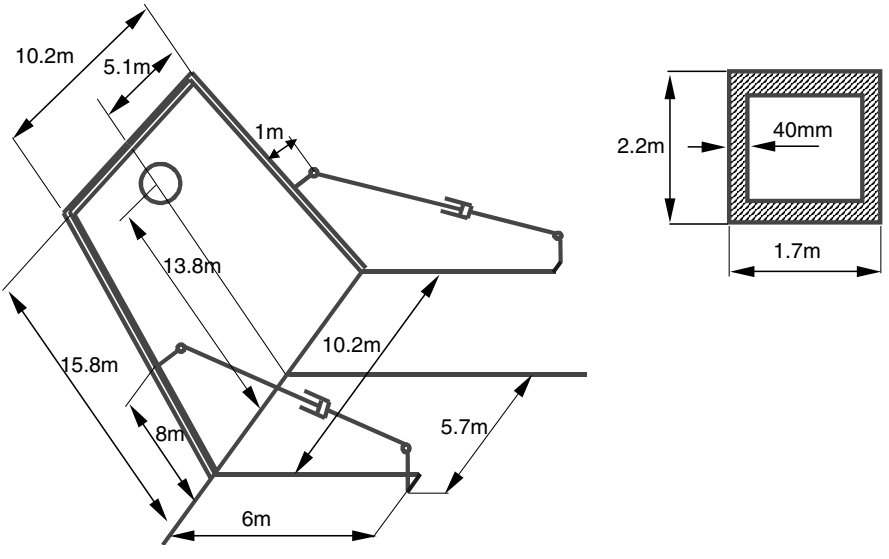

Fig. 10.11. Geometrical parameters of the A-frame

In the figures the following denotations are used: Ω_1, Ω_2 – curves obtained according to (10.37.1) and (10.37.2), respectively, S, H - curves obtained according to (10.39.1) and (10.39.2). Time courses of coordinate z_L obtained according to the full and the simplified model are shown in Fig. 10.12. In this case, the hoisting winch was motionless. The results of simulations are almost the same.

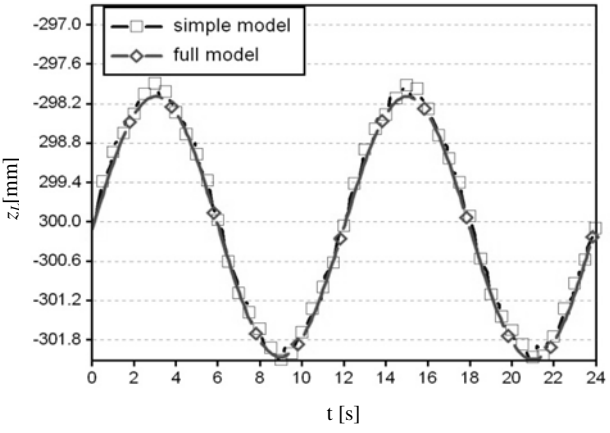

Fig. 10.12. Time courses of coordinates z_L

Because the simplified model is much more numerically efficient, the optimisation process has been solved for this model. Time courses of drive functions of the drum defined during the optimisation process are presented in Fig 10.13.

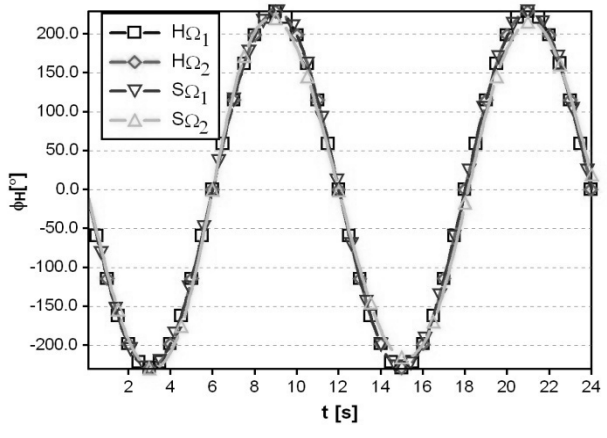

Fig. 10.13. Drive functions of drum after optimisation

As we can see, insignificant differences occurred between these drive functions. Drive functions obtained during optimisation have been taken as inputs of drum motion in the full model, so simulations presented below have been carried out according to the full model. Time courses of the coordinate z_L obtained when the drum of the hoisting winch was motionless and when its motion was determined by the function after optimisation (regardless of the type of the objective function and type of the drive function) are shown in Fig. 10.14. Amplitude of load oscillations has been decreased from 2 m to near zero.

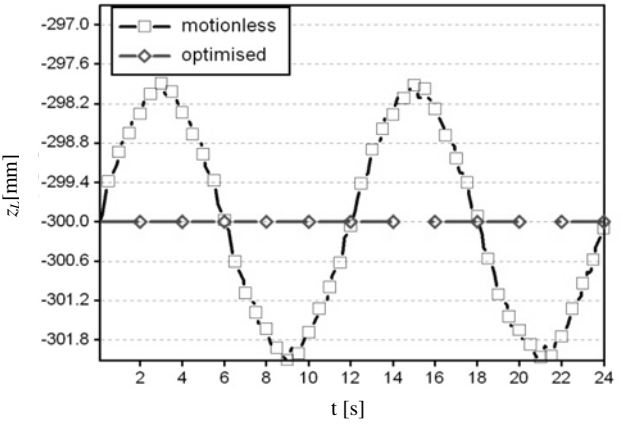

Fig. 10.14. Coordinate x_{L3} before and after optimisation

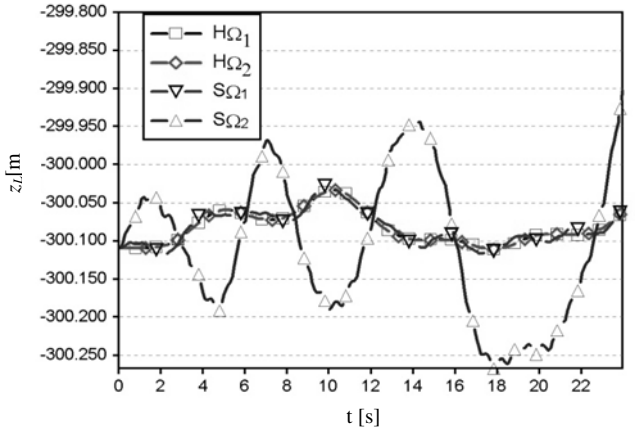

Fig. 10.15. Coordinate $x_{L,3}$ after optimisation for different type of objective and drive functions

Time courses of the coordinate z_L obtained for different types of objective functions and drive functions are presented in Fig. 10.15. The courses for the pseudo-harmonic drive function (10.38.2) and different types of objective functions are presented, in detail, in Fig. 10.16.

The model of an A-frame based on the finite element method has proved to be a useful instrument for carrying out dynamic analyses of this kind of cranes. This model is more numerically effective than the previous model presented in [Fałat P., 2004] (Fig. 10.3).

Numerical simulations presented in the chapter confirm the significant efficiency of the proposed method of optimisation drive function of the drum

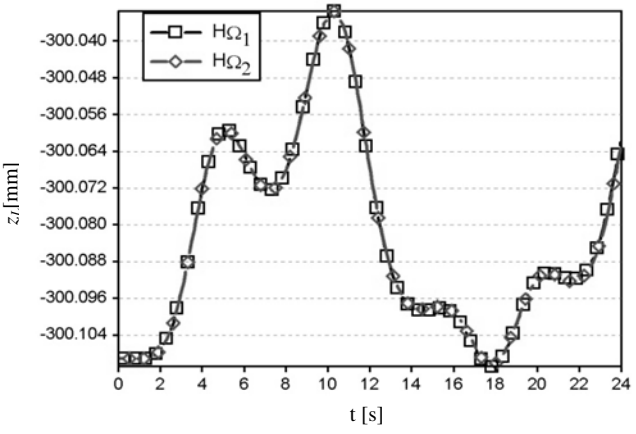

Fig. 10.16. Coordinate $x_{L,3}$ after optimisation for pseudo-harmonic drive function

where the main goal of the optimisation process is the stabilisation of the load position. Because the optimisation task has been carried out for the simplified model, the method is sufficiently effective.

For the motion of the ship discussed, the pseudo-harmonic drive functions are slightly better than spline functions. Amplitudes of load oscillations in the z_L direction are, for pseudo-harmonic functions, about 8 times smaller then for the spline function and the objective function Ω_1. When the objective function Ω_2 is taken, the results obtained are worst. However, when the system of waves is more complicated, the spline functions may be more useful.

Both objective functions, that is average and maximal value of deviation of load position from the demanded level, are acceptable in practice. There are no significant differences between results obtained for the two functions.

In real conditions, there are additional phenomena that can influence the quality of the stabilisation of the load position. There may be, for example, inaccurate definition of parameters of the crane. We should also remember that the rope interacts with the load and the environment mainly at low levels of depths, where water currents and waves are strong. Especially, in some conditions, a taut-slack phenomenon of a marine cable-body system can be significant [Huang S., 1999], [Jordan M. A., Bustamante J. L., 2007]. Vertical oscillations of the load induced by taut-slack phenomenon makes it more difficult to stabilise the load. An error-actuated control system for motion of the drum of the hoisting winch can minimise the impact of all those phenomena.

10.3 Stabilization of Crane Load with the Use of an Auxiliary System

In the present chapter, the authors take on the problem of load stabilization for a crane installed on a ship. The solution analyzed is inherently similar to the Knuckle Boom Telescopic Offshore Crane concept of TTS-Aktro. The base of the

crane (i.e. the ship) is subject to general type of motion as a rigid body whose components are defined by pseudo-harmonic functions. Two dynamical models of a crane have been developed: a simplified one, suitable for determining drive functions, and a basic one, for which more accurate dynamical analyses are possible. Furthermore, two methods of determining drive functions of the crane's mechanisms ensuring stabilization of load's position are proposed. The first one involves solving the inverse kinematics problem for quasi-static conditions, the second one is based on dynamic optimization. Results of sample numerical simulations are included.

10.3.1 Auxiliary System for Stabilization of Load Position

Complete stabilization of load's position requires the ability to exert force on the load in three independent directions. In the vertical direction it is natural to use the hoisting winch drum's drive. For the stabilization in two remaining directions, the authors propose using an additional auxiliary system (Fig. 10.17). Its main component is a stiff element leading the rope along the GD segment. By inclining this element it is possible to move the point D of the hoist rope in two directions: tangential (τ) and radial (n). The directions τ and n have been defined relative to the trajectory of point G of the jib in its rotating motion. Dislocating point D is the means for influencing the load's motion and thus an attempt to stabilize it in the aforementioned directions becomes feasible. The proposed solution has the advantage of being applicable to stabilization of load's position or, when another strategy is selected, to other tasks, e.g. limiting swaying of the load during rotating movement of the crane's upper structure.

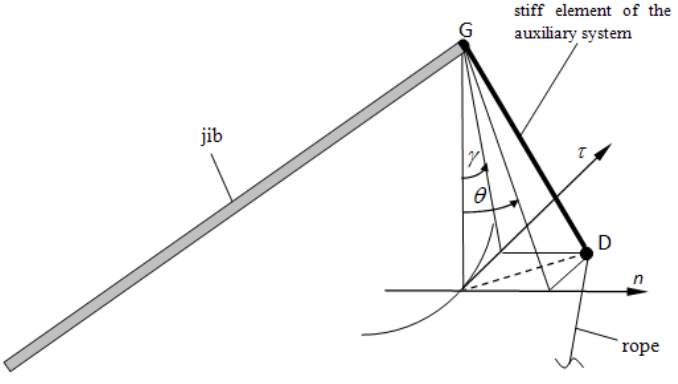

Fig. 10.17. Auxiliary system reducing load oscillations

10.3.2 Models of an Offshore Crane with the Auxiliary System

Depending on the purpose models of equipment are built which vary in complexity. Thus they represent the dynamic properties of the modelled object with different fidelity. In problems of control the speed of computation is very important. Real-time control is often required. This leads to possibly simple models being used which enable numerical efficiency. On the contrary, when the model is to be suitable for asserting validity of the equipment's operation, its basic dynamical behaviour must be reflected more accurately. Accuracy of the results obtained and their correspondence to reality is much more important than the time of computation in this case.

The authors have developed two models of an offshore crane with the auxiliary system: a simplified one, suitable for determining drive functions, and a basic one, for which more accurate dynamical analyses are possible. Simulations using the basic model enabled carrying out tests to confirm the suitability of the method proposed to the problem of load's position stabilization. In Table 10.1, there are compared the basic properties of both models. An outlined scheme of the simplified model is shown in Fig. 10.18.

The equations of motion in the basic model have been derived along the lines of [Wittbrodt E., et al., 2006] and [Adamiec-Wójcik I., et al., 2008]. Lagrange's equations of the second order have been used. The vector **q** of the generalized coordinates can be written as:

$$\mathbf{q} = \left[\mathbf{q}^{(A)^T} \quad \varphi \quad \psi \quad \mathbf{q}^{(J)^T} \quad \alpha \quad \gamma \quad \theta \quad \mathbf{q}^{(L)^T}\right]^T, \tag{10.44}$$

where $\mathbf{q}^{(A)} = \left[x_{org}^{(A)} \quad y_{org}^{(A)} \quad z_{org}^{(A)} \quad \varphi^{(A)} \quad \theta^{(A)} \quad \psi^{(A)}\right]^T$ – vector of generalized coordinates of the base (deck),

$\mathbf{q}^{(J)} = \left[q_1^{(J)} \quad \ldots \quad q_k^{(J)} \quad \ldots \quad q_m^{(J)}\right]^T$ – vector of generalized coordinates of the jib,

$\mathbf{q}^{(L)} = \left[x_L \quad y_L \quad z_L\right]^T$ – vector of generalized coordinates of the load,

φ – rotation angle of the crane's pedestal (upper structure) – slewing angle,

ψ – inclination angle of the undeformed jib,

α – rotation angle of the hoisting winch's drum.

γ, θ – angles of inclination of auxiliary system (Fig. 10.18).

Relationships which determine individual terms of the Lagrange's equations are obtained similarly as in the case of a mobile crane treated in [Maczyński A., Wojciech S., 2003].

To ensure that the crane's base moves according to the provisions of Table 10.1, the following condition must hold:

$$q_i^{(A)} = \alpha_i^{(A)}(t) \qquad \text{for } i = 1,...,6. \tag{10.45}$$

Table 10.1. Comparison of models: simplified and basic

	Simplified model	Basic model
Form of description for system's points	absolute coordinates	coordinates relative to joints
Method of obtaining equations of motion	second Newton's law	Lagrange's equations of second order
Number of degrees of freedom	3	14+m where m is the total number of modes considered in the jib's model
Drives considered	1. hoisting winch drum's 2. auxiliary system's in directions τ and n	1. hoisting winch drum's 2. auxiliary system's in directions τ and n 3. of crane's upper structure's slewing 4. of reach changing (reach changing actuator)
Drive modeling method	kinematic driving	kinematic driving by a parallel system of a spring and a damper
Pedestal	modeled as a rigid body, fixed to the base (ship's deck)	
Load	modeled as an concentrated mass	
Rope	flexible	flexible with damping
Jib	rigid	capable of flexing – the jib has been discretized using modal method
Description of base's motion	pseudo-harmonic: $\alpha_i^{(A)} = \sum_{j=1}^{n_i^{(A)}} A_{i,j}^{(A)} \sin(\omega_{i,j}^{(A)} t + \varphi_{i,j}^{(A)})$ for $i = 1,\ldots,6$, where $\left[\alpha_1^{(A)} \quad \ldots \quad \alpha_6^{(A)}\right]^T = \left[x_{org}^{(A)} \quad y_{org}^{(A)} \quad z_{org}^{(A)} \quad \varphi^{(A)} \quad \theta^{(A)} \quad \psi^{(A)}\right]^T = \boldsymbol{\alpha}$ $A_{i,j}^{(A)}$ - j^{th} amplitude in the i^{th} direction, $\omega_{i,j}^{(A)}$ - j^{th} angular frequency in the i^{th} direction, $\varphi_{i,j}^{(A)}$ - j^{th} phase angle in the i^{th} direction.	
Equations of motion	$\begin{cases} m_L \ddot{x}_L = S\dfrac{x_D - x_L}{L_{DL}} + F_X + T_X \\ m_L \ddot{y}_L = S\dfrac{y_D - y_L}{L_{DL}} + F_Y + T_Y \\ m_L \ddot{z}_L = S\dfrac{z_D - z_L}{L_{DL}} + F_Z + T_Z - m_L g \end{cases}$ where $S = c_l(L_{DL} + L_D - L_0 + \alpha \cdot r_B) + b_l(\dot{L}_{DL} + \dot{\alpha} \cdot r_B)$, $L_{DL}^2 = (x_D - x_L)^2 + (y_D - y_L)^2 + (z_D - z$, c_l, b_l – stiffness and damping coefficients of the rope, respectively, α – rotation angle of the hoisting winch's drum, r_B – radius of the hoisting winch's drum, L_0 – initial length of the rope.	Described later
Integration method for the equations of motion	Runge-Kutta method of fourth order	

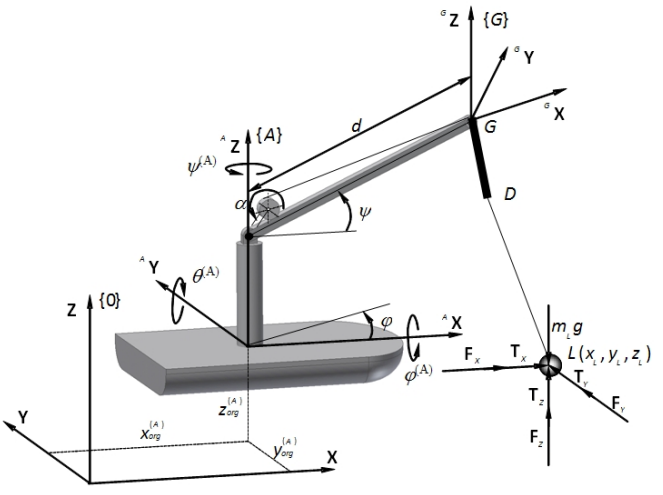

Fig. 10.18. Simplified model of an offshore crane

Forces and moments of force acting on the crane's base to make it move according to relationships (10.45) must be therefore introduced into the system. They are assumed to form the following vector:

$$\mathbf{R}^{(A)} = \left[F_x^{(A)}, F_y^{(A)}, F_z^{(A)}, M_x^{(A)}, M_y^{(A)}, M_z^{(A)}\right]^T . \tag{10.46}$$

Forces and moments of force are depicted in Fig. 10.19.

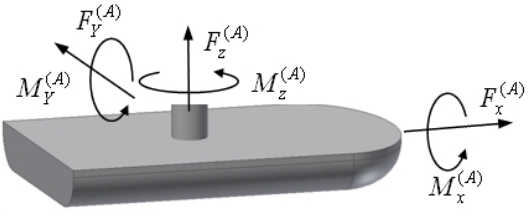

Fig. 10.19. External forces and their moments acting on the crane's base

The model of an offshore crane is ultimately described by the following equations of motion:

$$\mathbf{A}\ddot{\mathbf{q}} - \mathbf{D}\mathbf{R}^{(A)} = \mathbf{F} , \tag{10.47}$$

where $\mathbf{A}$ – mass matrix,
$\mathbf{R}^{(A)}$ – vector defined in (10.46),

$$\mathbf{D} = \begin{bmatrix} \mathbf{I}_{6\times 6} \\ \mathbf{0}_{m\times 6} \end{bmatrix},$$

$\overline{m} = 14 + m - 6$,

$\mathbf{I}_{6\times6}$ – identity matrix of dimension 6x6,

$\mathbf{F}$ – vector on the right side of the equation of motion including among others the terms of Lagrange's equation related to velocities and generalized coordinates as well as non-potential forces not accounted for in vector $\mathbf{R}^{(A)}$,

which must be supplemented by constraint equations:

$$\mathbf{q}^{(A)} = \boldsymbol{\alpha}^{(A)}. \tag{10.48}$$

10.3.3 Drive Functions Stabilizing Load's Position: The Inverse Kinematics Problem

The first of the methods considered by the authors to determine drive functions which ensure stabilization of crane load's position is solving the inverse kinematics problem for quasi-static conditions. This task consists in choosing functions for the auxiliary system's and hoisting winch drum's motions so that the load stays in its initial position when the motion of the crane's base is taken into account. However, dynamic effects are not considered.

Before the desired drive functions can be determined, it is necessary to set the initial position of the mass m_L, i.e. the initial values of the coordinates x_L^0, y_L^0, z_L^0 that they have at the beginning of the stabilization. They provide the initial conditions for the problem of determining drive functions in quasi-static conditions. The equations of static equilibrium for the simplified model are:

$$\begin{aligned} f_1 &= x_D - x_L + \frac{L_{DL}}{S} F_X = 0 \\ f_2 &= y_D - y_L + \frac{L_{DL}}{S} F_Y = 0 \\ f_3 &= z_D - z_L + \frac{L_{DL}}{S}\left(F_Z - m_L g\right) = 0 \end{aligned}, \tag{10.49}$$

where $S = c_L\left[L_{DL} + L_D - L_0 + \alpha^0 r_B\right]$,

$L_{DL} = \sqrt{(x_D - x_L)^2 + (y_D - y_L)^2 + (z_D - z_L)^2}$,

$c_l = \dfrac{E_r A_R}{L_0 - \alpha\, r_B}$,

E_r – Young's modulus,

$r_B(t)$ – radius of the drum,

A_r – cross-sectional area of the rope.

Coordinates x_D, y_D, z_D can be obtained from:

$$\mathbf{r_D} = \begin{bmatrix} x_D \\ y_D \\ z_D \\ 1 \end{bmatrix} = \mathbf{T_P}\ \mathbf{T_G} \begin{bmatrix} x_D' \\ y_D' \\ z_D' \\ 1 \end{bmatrix} = \mathbf{T}\,\mathbf{r_D'}, \tag{10.50}$$

where $z_D' = \dfrac{L_D \cos\theta \cos\gamma}{\sqrt{1-\sin^2\theta \sin^2\gamma}}$,

$x_D' = z_D' tg\,\theta$,

$y_D' = z_D' tg\,\gamma$,

$\mathbf{r_D'} = \left[x_D', y_D', z_D', 1\right]^T$,

$\mathbf{T_P}$ – transformation matrix from {P} coordinate system to the inertial coordinate system {0},

$\mathbf{T_G}$ – transformation matrix from {G} to {P} coordinate systems.

The matrices $\mathbf{T_P}$ and $\mathbf{T_G}$ appearing in (10.50) are defined as:

$$\mathbf{T_P} = \mathbf{T_P}(t) = \begin{bmatrix} \mathbf{R_P} & \mathbf{r_P} \\ \mathbf{0} & 1 \end{bmatrix}, \tag{10.51}$$

$$\mathbf{T_G} = \begin{bmatrix} c\varphi & s\varphi & 0 & d\,c\psi\,c\varphi \\ s\varphi & -c\varphi & 0 & d\,c\psi\,s\varphi \\ 0 & 0 & -1 & d\,s\psi \\ 0 & 0 & 0 & 1 \end{bmatrix} = const, \tag{10.52}$$

where d – length of the jib (Fig. 10.18),

$$\mathbf{R_P} = \begin{bmatrix} c\psi^{(A)} & -s\psi^{(A)} & 0 \\ s\psi^{(A)} & c\psi^{(A)} & 0 \\ 0 & 0 & 1 \end{bmatrix} \begin{bmatrix} c\theta^{(A)} & 0 & s\theta^{(A)} \\ 0 & 1 & 0 \\ -s\theta^{(A)} & 0 & c\theta^{(A)} \end{bmatrix} \begin{bmatrix} 1 & 0 & 0 \\ 0 & c\varphi^{(A)} & -s\varphi^{(A)} \\ 0 & s\varphi^{(A)} & c\varphi^{(A)} \end{bmatrix},$$

$$\mathbf{r_P} = \begin{bmatrix} x_P \\ y_P \\ z_P \end{bmatrix},$$

$c\varphi = \cos\varphi, \quad s\varphi = \sin\varphi$.

The unknown values of the coordinates x_L^0, y_L^0, z_L^0 are determined from (10.50) assuming $t = t_0$, $\alpha = \alpha^0, \theta = \theta^0$ and $\gamma = \gamma^0$, where $t_0, \alpha^0, \theta^0, \gamma^0$ are, respectively, the initial time (moment) of starting the stabilization and the values

of angles α, γ, θ at the time $t = t_0$. Equations (10.50) form a system of 3 nonlinear equations with 3 unknowns $x_L = x_L^0$, $y_L = y_L^0$, $y_L = y_L^0$, which is solved with Newton's iteration method.

Having determined $x_L = x_L^0$, $y_L = y_L^0$ and $z_L = z_L^0$, the procedure continues determining the drive functions for quasi-static conditions. Let:

$$t_i = t_0 + i\Delta t \qquad i = 1,...,p, \quad (10.53)$$

where $\Delta t = \dfrac{t_k - t_0}{p}$,

t_k – end time of load stabilization,

p – number of intervals into which the time interval $\langle t_0, t_k \rangle$ has been divided.

Assuming that the following conditions must hold at time $t = t_1,...,t_p$:

$$\begin{aligned} x_L\big|_{t=t_i} &= x_L^0 \\ y_L\big|_{t=t_i} &= y_L^0 \\ z_L\big|_{t=t_i} &= z_L^0 \end{aligned} \qquad i = 1,...,p, \qquad (10.54)$$

equations (10.49) of static equilibrium for $t = t_i$ can be written as:

$$\begin{aligned} f_1\left(\alpha^{(i)}, \theta^{(i)}, \gamma^{(i)}\right) &= x_D - x_L^0 + \frac{L_{DL}}{S} F_X = 0 \\ f_2\left(\alpha^{(i)}, \theta^{(i)}, \gamma^{(i)}\right) &= y_D - y_L^0 + \frac{L_{DL}}{S} F_Y = 0 \\ f_3\left(\alpha^{(i)}, \theta^{(i)}, \gamma^{(i)}\right) &= z_D - z_L^0 + \frac{L_{DL}}{S}\left(F_Z - m_L\, g\right) = 0 \end{aligned} \qquad i = 1,...,p, \quad (10.55)$$

where $\mathbf{r_D} = \begin{bmatrix} x_D \\ y_D \\ z_D \\ 1 \end{bmatrix} = \mathbf{T^{(i)}} \begin{bmatrix} x_D' \\ y_D' \\ z_D' \\ 1 \end{bmatrix} = \mathbf{T^{(i)}}\, \mathbf{r_D'}$,

$\mathbf{T^{(i)}} = \mathbf{T}(t_i)$,

S – defined in (10.49).

Equations (10.55) form a system of $3p$ nonlinear algebraic equations with $3p$ unknowns $\alpha^{(i)}$, $\gamma^{(i)}$, $\theta^{(i)}$. These equations have also been solved by applying Newton's iteration method taking the starting point for subsequent iterations to be:

$$\begin{aligned}\alpha^{(i),0} &= \alpha^{(i-1)} \\ \gamma^{(i),0} &= \gamma^{(i-1)} \\ \theta^{(i),0} &= \theta^{(i-1)}\end{aligned}, \tag{10.56}$$

The continuous functions $\alpha = \alpha(t),\ \gamma = \gamma(t),\ \theta = \theta(t)$ have been obtained by connecting points with splines.

As it has been described above, the courses angles of the hoisting winch and the auxiliary system are calculated using the simplified model and omitting dynamic phenomena. However, these courses compensating sea waves can be successfully applied in dynamic simulations using both models. The further calculations are carried out using the basic model of the crane. The crane is assumed to have a 14 m long jib and an L_D = 5 m long auxiliary system. The angle ψ was 50°, the load's mass 10000 kg, its z coordinate -20 m. For this data, the distance from point G of the jib to the load is 31.75 m. Although, as previously mentioned, offshore cranes usually operate from watercrafts conveniently positioned against waves, a general motion of the base has been considered for sample excitations. The results follow [Balachandran B., et al., 1999]:

$$\begin{aligned}
x_{org}^{(D)} &= 0.6\left(\sin 0.52t + \frac{1}{4}\sin 1.04t + \frac{1}{9}\sin 1.56t\right)[\mathrm{m}], \\
y_{org}^{(D)} &= 0.6\left(\sin(0.52t + 3.14) + \frac{1}{4}\sin(1.04t + 3.14) + \frac{1}{9}\sin(1.56t + 3.14)\right)[\mathrm{m}], \\
z_{org}^{(D)} &= 1.2\left(\sin(0.52t + 3.14) + \frac{1}{4}\sin(1.04t + 3.14) + \frac{1}{9}\sin(1.56t + 3.14)\right)[\mathrm{m}], \\
\varphi^{(D)} &= 3\left(\sin(0.52t + 3.14) + \frac{1}{4}\sin(1.04t + 3.14) + \frac{1}{9}\sin(1.56t + 3.14)\right)[^{\circ}], \\
\theta^{(D)} &= 5\left(\sin 0.52t + \frac{1}{4}\sin 1.04t + \frac{1}{9}\sin 1.56t\right)[^{\circ}], \\
\psi^{(D)} &= 5\left(\sin 0.52t + \frac{1}{4}\sin 1.04t + \frac{1}{9}\sin 1.56t\right)[^{\circ}].
\end{aligned} \tag{10.57}$$

By the assumption of such motion of the crane's base, the analysis of the general case was possible to perform, which required using auxiliary system's drives in both directions: radial and tangential. The time of stabilization (observation of the load) was 60 s. The coordinates x, y, z of the load, respectively, for the auxiliary system and hoisting winch's drum both idle and controlled according to the drive functions determined are shown in Figs. 10.20, 10.21 and 10.22. Time courses of dynamic coefficient of the force in the rope for both cases are presented in Fig. 10.23. The dynamic coefficient is defined as:

$$\eta = \frac{S}{m_L\, g}, \tag{10.58}$$

where S is the force in the rope.

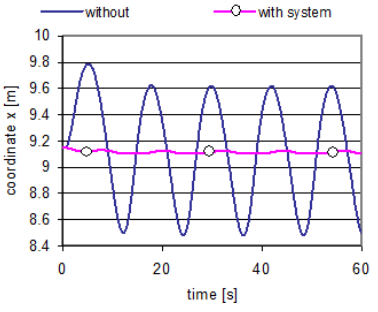

Fig. 10.20. Time course of x_L coordinate for general motion of the base

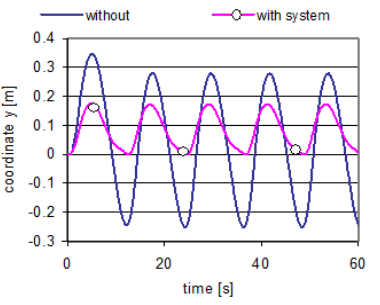

Fig. 10.21. Time course of y_L coordinate for general motion

The results obtained show that using the proposed method yields highly effective stabilization of the load. The outstanding quality of stabilization along the axes **X** and **Z** is worth emphasizing. Stabilizing the load's position has also decreased the dynamic coefficient of the force in the rope, thus alleviating dynamic strains in the crane's structure.

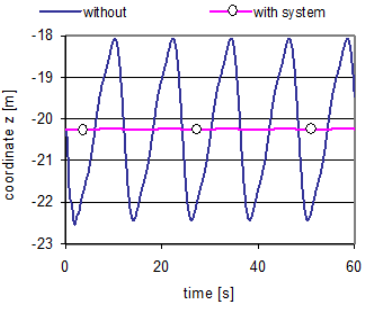

Fig. 10.22. Time course of z_L coordinate for general motion

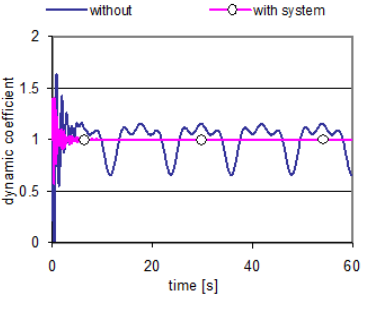

Fig. 10.23. Time course of the dynamic coefficient

10.3.4 Optimizing Drive Functions

Optimization is a method often applied in determining drive functions for a range of mechanisms and machines. Naturally, the optimization criteria may vary. Some examples are: minimal duration of motion, minimal energy consumption, minimal dynamic strains, approximating desired trajectories for selected points, etc.

In the considered case of stabilizing offshore crane load's position, the optimization task is to determine the functions $\alpha = \alpha(t)$, $\gamma = \gamma(t)$, $\theta = \theta(t)$, so that despite the crane base's motion (i.e. despite the variability of the matrix $\mathbf{T}(t)$

of (10.50)) the load remains possibly close to its initial position. Hence the definition of the goal function:

$$\Omega(\alpha,\gamma,\theta)=\int_{t_0}^{t_k}\left[\left(x_L-x_L^0\right)^2+\left(y_L-y_L^0\right)^2+\left(z_L-z_L^0\right)^2\right]dt\ , \tag{10.59}$$

where $x_L^0,\ y_L^0,\ z_L^0$ are initial coordinates of the load determined as in the previous section, from (10.49).

Since it has been assumed that the crane base's motion is defined by pseudo-harmonic functions, it seems natural to seek the drive functions $\alpha=\alpha(t),\ \gamma=\gamma(t),\ \theta=\theta(t)$ of the from:

$$\begin{aligned}\alpha&=\alpha^0+\sum_{i=1}^{n_\alpha}A_{\alpha,i}\sin\left(\omega_{\alpha,i}t+\varphi_{\alpha,i}\right)\\ \gamma&=\gamma^0+\sum_{i=1}^{n_\gamma}A_{\gamma,i}\sin\left(\omega_{\gamma,i}t+\varphi_{\gamma,i}\right)\ ,\\ \theta&=\theta^0+\sum_{i=1}^{n_\theta}A_{\theta,i}\sin\left(\omega_{\theta,i}t+\varphi_{\theta,i}\right)\end{aligned} \tag{10.60}$$

where $\alpha^0,\gamma^0,\theta^0$ – initial values of angles α,γ,θ,

$A_{j,i},\omega_{j,i},\varphi_{j,i}$ – i^{th} amplitude, angular frequency and phase angle of the j^{th} drive, satisfying $j\in\{\alpha,\gamma,\theta\}$.

Decision variables of an optimization task thus stated can be written as vectors:

$$\mathbf{X}_\alpha=\begin{bmatrix}\mathbf{X}_{\alpha,1}\\ \vdots\\ \mathbf{X}_{\alpha,\mathbf{i}}\\ \vdots\\ \mathbf{X}_{\alpha,\mathbf{n}_\alpha}\end{bmatrix}\ ,\quad \mathbf{X}_{\alpha,\mathbf{i}}=\begin{bmatrix}A_{\alpha,i}\\ \omega_{\alpha,i}\\ \varphi_{\alpha,i}\end{bmatrix}\qquad \mathrm{i}=1,\ldots,n_\alpha, \tag{10.61}$$

$$\mathbf{X}_\gamma=\begin{bmatrix}\mathbf{X}_{\gamma,1}\\ \vdots\\ \mathbf{X}_{\gamma,\mathbf{i}}\\ \vdots\\ \mathbf{X}_{\gamma,\mathbf{n}_\gamma}\end{bmatrix}\ ,\quad \mathbf{X}_{\gamma,\mathbf{i}}=\begin{bmatrix}A_{\gamma,i}\\ \omega_{\gamma,i}\\ \varphi_{\gamma,i}\end{bmatrix}\qquad \mathrm{i}=1,\ldots,n_\gamma, \tag{10.62}$$

$$\mathbf{X}_{\theta} = \begin{bmatrix} \mathbf{X}_{\theta,1} \\ \vdots \\ \mathbf{X}_{\theta,i} \\ \vdots \\ \mathbf{X}_{\theta,n_\theta} \end{bmatrix} \quad , \quad \mathbf{X}_{\theta,i} = \begin{bmatrix} A_{\theta,i} \\ \omega_{\theta,i} \\ \varphi_{\theta,i} \end{bmatrix} \qquad i = 1,...,n_\theta , \tag{10.63}$$

and finally:

$$\mathbf{X} = \begin{bmatrix} \mathbf{X}_{\alpha} \\ \mathbf{X}_{\gamma} \\ \mathbf{X}_{\theta} \end{bmatrix} . \tag{10.64}$$

Vector (10.64) has:

$$n = 3\left(n_\alpha + n_\gamma + n_\theta\right) \tag{10.65}$$

coordinates. The optimization consists in determining such combination of decision variables satisfying these constraints:

$$\begin{array}{lll} A_{\alpha,i,\min} \le A_{\alpha,i} \le A_{\alpha,i,\max} & A_{\gamma,i,\min} \le A_{\gamma,i} \le A_{\gamma,i,\max} & A_{\theta,i,\min} \le A_{\theta,i} \le A_{\theta,i,\max} \\ \omega_{\alpha,i,\min} \le \omega_{\alpha,i} \le \omega_{\alpha,i\max} & \omega_{\gamma,i,\min} \le \omega_{\gamma,i} \le \omega_{\gamma,i\max} & \omega_{\theta,i,\min} \le \omega_{\theta,i} \le \omega_{\theta,i\max} \\ \varphi_{\alpha,i,\min} \le \varphi_{\alpha,i} \le \varphi_{\alpha,i,\max} & \varphi_{\gamma,i,\min} \le \varphi_{\gamma,i} \le \varphi_{\gamma,i,\max} & \varphi_{\theta,i,\min} \le \varphi_{\theta,i} \le \varphi_{\theta,i,\max} \end{array} , \tag{10.66}$$

that the goal function (10.59) attains its minimal value.

To calculate the goal function, the coordinates x_L, y_L, z_L must be defined. This requires integration of the crane model's equations of motion for $t \in \langle t_0, t_k \rangle$. As mentioned before, to achieve reasonable numerical efficiency the optimization task was solved using the simplified model. Nelder-Mead simplex method was employed for the optimization [Wit R., 1986].

Judicious choice of initial approximations of functions to optimize is an important requirement. They should already be near the solution. The case of pseudo-harmonic functions involves an additional difficulty in selecting the number of harmonic components, i.e. the values $n_\alpha, n_\gamma, n_\theta$. This problem is briefly accounted for in the following. The initial approximation was chosen to be defined as a sum of n_j harmonic components ($j \in \{\alpha, \gamma, \theta\}$) obtained from Fourier analysis applied to drive functions which are the solutions of the inverse kinematics problem for quasi-static conditions. It should be clearly stated that the method proposed for determining optimized drive functions requires that they be preset with the procedure of chaper 10.3.3 beforehand.

With Fourier analysis [Kruszewski J., Wittbrodt E., 1992], an arbitrary periodic function can be represented as a series:

$$x(t) = x_0^0 + \sum_{\nu=1}^{l} x_\nu^o \sin\left(\nu\,\omega t + \varphi_{x\nu}\right), \tag{10.67}$$

where l – number of terms (harmonic components) in the series,
ν – index of harmonic component,
t – time,
x_0^0 – constant term of the series,
$x_\nu^0, \varphi_{x\nu}$ – amplitude and phase angle of the ν^{th} component, respectively,
$\omega = \dfrac{2\pi}{T}$ – lowest angular frequency,
T – function's period.

Individual coefficients of a Fourier series are given by the following formulae:

$$x_0^0 = \frac{1}{N}\sum_{i=0}^{N-1} x_i \,, \tag{10.68}$$

$$x_\nu^0 = \sqrt{a_\nu^2 + b_\nu^2} \,, \tag{10.69}$$

$$\varphi_\nu^0 = arctg\left(\frac{a_\nu}{b_\nu}\right), \tag{10.70}$$

where $a_\nu = \dfrac{2}{N}\sum_{i=0}^{N-1} x_i \cos\dfrac{2\pi\,\nu\,i}{N},$

$b_\nu = \dfrac{2}{N}\sum_{i=0}^{N-1} x_i \sin\dfrac{2\pi\,\nu\,i}{N},$

$\nu = 1,2,...,l,$

N – number of sampling points for the function $x(t)$,

whereas l, the number of harmonic components, must satisfy this condition:

$$2l + 1 < N \,. \tag{10.71}$$

The hoisting winch drum's drive may obviously have different number of harmonic components in the initial approximation from either radial or tangential direction of the auxiliary system. It is, however, natural to assume that the number of components present in the initial approximation remains the same in the optimized function.

Drive functions optimized using different numbers of harmonic components (n_j = 2 and n_j = 4) with the method of chaper 10.3.3 (being the input of Fourier analysis) are compared below to their initial approximations. Parameters describing geometry and mass distribution of the crane were identical to those considered in chaper 10.3.3 and the excitation of the base was given by (10.57). The graphs in Figs. 10.24, 10.25 are for the drive function of the hoisting winch's drum, those in Figs. 10.26, 10.27 for the rotation of the auxiliary system's rigid component in the radial plane and those in Figs. 10.28 and 10.29 in the tangential plane.

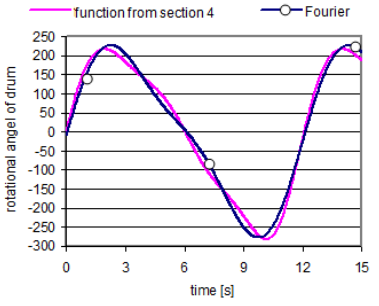

Fig. 10.24. Comparison of the hoisting winch drum's analytic drive function and its initial approximation (2 components)

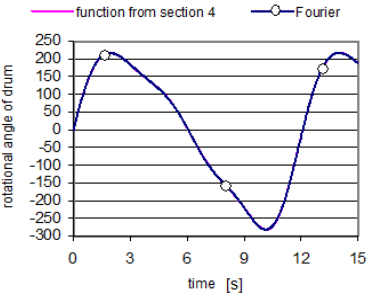

Fig. 10.25. Comparison of the hoisting winch drum's analytic drive function and its initial approximation (4 components)

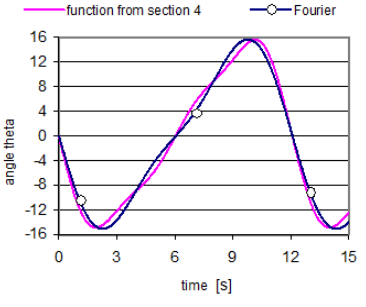

Fig. 10.26. Comparison of the θ angle's analytic drive function and its initial approximation (2 components)

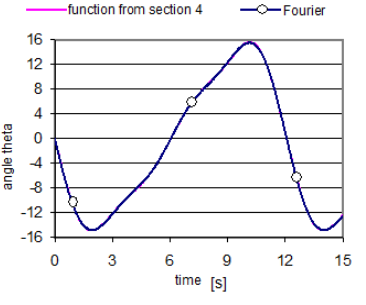

Fig. 10.27. Comparison of the θ angle's analytic drive function and its initial approximation (4 components)

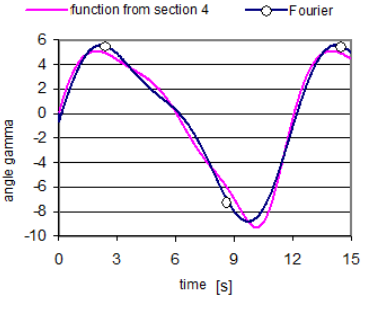

Fig. 10.28. Comparison of the γ angle's analytic drive function and its initial approximation (2 components)

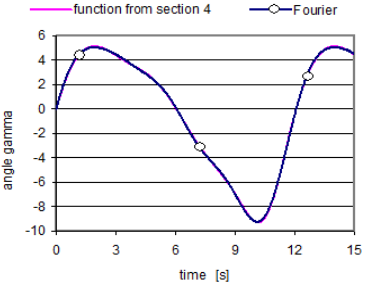

Fig. 10.29. Comparison of the γ angle's analytic drive function and its initial approximation (4 components)

As it can be seen, taking $n_j = 4$ leads to very good approximation of drive functions with a Fourier series. Thence follows reasonableness of seeking the initial approximation in the class of functions of the form (10.60).

Next, stabilization of load's position was considered for durations of 20 and 60 s. The value of the goal function (10.59) for idle auxiliary system and hoisting winch's drum was 47.07 for stabilization time 20 s and 142.10 for 60 s. Comparison of the goal function's values for initial approximations and their corresponding optimized drive functions for different numbers of harmonic components are presented in Table 10.2. Number of iterations and time of computation used by the optimization process are also compared.

Table 10.2. Comparison of the goal function's values

Duration of stabilization [s]	Number of components			Value of the goal function		Number of iterations	Approximated computation time taken by the optimization
	hoisting winch's drum	θ angle	γ angle	initial approxi-mation	optimized function		
20	2	2	2	0.579625	0.388667	3053	6.5 min
20	4	4	4	0.000571	0.000208	3835	9 min
20	6	6	6	0.000054	0.000011	10894	33 min
60	2	2	2	1.677738	1.226042	1699	13 min
60	4	4	4	0.001667	0.000555	3673	27 min
60	6	6	6	0.000121	0.000490	10369	85 min

The results presented (of calculations for the simplified model) made it possible to draw the following conclusions:

- in the Fourier analysis taking into consideration 4 harmonic components is sufficient for obtaining satisfying drive functions determined for quasi-static conditions,
- initial approximations stabilize the load's position well; indeed, taking as few as 2 harmonic components of each initial approximation gives a reduction of the goal function's value by a factor of about 100 compared to the case of idle hoisting winch's drum and auxiliary system,
- substantial influence of the number of components in the initial approximation on the quality of stabilization is clearly noticeable,
- only slightly does optimization improve stabilization of the load.

These conclusions led the authors to abandoning further work with the idea of determining drive functions for stabilization of load's position using optimization.

The reason is that the process is lengthy, requires determining drive functions for quasi-static conditions, and the improvement obtained in the quality of load stabilization is modest.

We would like to underlain that above conclusions are valid only for the assumed pseudo-harmonic base motion. In the case of more complicated functions defining base motion, the second approach, when optimization methods are applied, seems to be better, since it is more general. The decision variable could be the values of spline functions defining drives [Maczyński A., Wojciech S., 2003].

10.3.5 Control System

The proposed system of stabilization of load's position could be augmented with a closed-loop control system. Its task would be to minimize the influence of the jib and the hoisting system's flexibility neglected in the model, of inaccurate knowledge of parameters describing the geometry and mass distribution of the crane as well inaccurate knowledge of waves parameters, eventually of potential external disturbances.

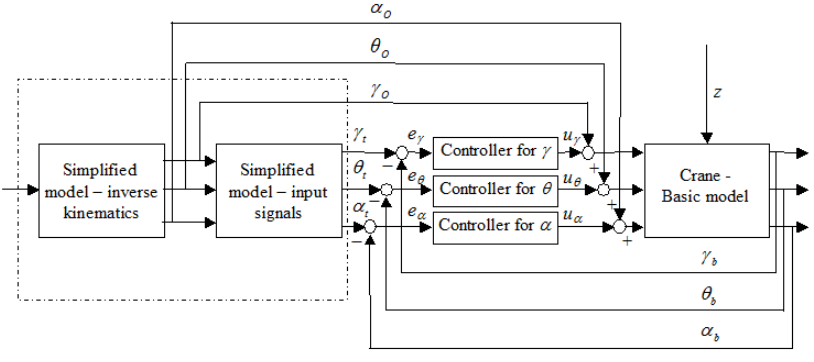

Fig. 10.30. Block diagram of control system: γ_O, θ_O, α_O – drive functions determined according the simplified model, γ_t, θ_t, α_t – input signals determined according the simplified model, γ_b, θ_b, α_b – current values of controlled signals, e_γ, e_θ, e_α – dynamic errors, u_γ, u_θ, u_α – output signals, z – disturbance

A block diagram of the considered control system is shown in Fig. 10.30. Three independent controllers, one for rotation of the drum and two for rotational motions of the stiff element of the auxiliary system, are used. The control system contains feed-back loops as well feed-forward loops. Time courses of the inputs signals ($\alpha_t = \alpha_t(t)$, $\gamma_t = \gamma_t(t)$, $\theta_t = \theta_t(t)$) have to be determined simultaneously with the drive functions ($\alpha_0 = \alpha_0(t)$, $\gamma_0 = \gamma_0(t)$, $\theta_0 = \theta_0(t)$) according to the simplified model. It is worth to be mentioned that in a standard stabilization task the following relationships are fulfilled:

$$\begin{aligned} \alpha_t(t) &= z_L^0 = const \\ \gamma_t(t) &= y_L^0 = const \\ \theta_t(t) &= x_L^0 = const \end{aligned} . \tag{10.72}$$

Time courses of load coordinates, x_L, y_L, z_L respectively, for waves increased about 10% in relation to the nominal defined in (10.57), are shown in Figs. 10.31, 10.32 and 10.33. Numerical calculations were carried out according to the basic model, drive functions were determined from chaper 10.3.3. Two cases were considered: with and without control system. The P controller was used in analyzed control system. The obtained results are very promising.

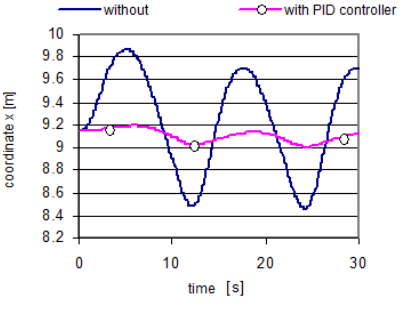

Fig. 10.31. Time course of xL coordinate

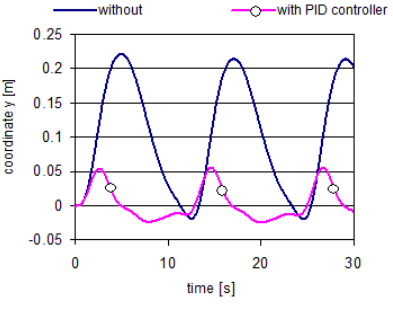

Fig. 10.32. Time course of y_L coordinate

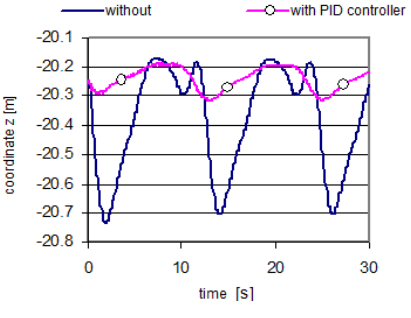

Fig. 10.33. Time course of z_L coordinate

10.4 Active Waves Compensation System for the Reel's Drive

Practice and the results of numerical simulations (chapter 9.3) show that during operation of a reel device for laying pipelines under sea waves its uneven work may occur. To reduce this undesirable effect, a modification of the reel's drive system is proposed. In place of a passive system (in which the braking force of the reel is a constant set by the operator) an active system may be installed with

controllable value of the force. That value would be chosen so that the moment maintains the assumed velocity of the reel and constant tension in the pipeline despite the occurrence of additional dynamic loads caused by sea waves. That would be a new solution, as yet unseen in existing drives, however, it would require a change of the way the drive system is designed: the engines (hydraulic or electric) would need the ability of exerting moments in both directions (classical passive systems are only capable of braking the reel during normal operation). The concept is discussed in details by [Szczotka M., 2010], [Szczotka M., 2011b].

10.4.1 Model of the Control System

Frequency converters are commonly used to control velocity and drive moment of electric engines [Olsson G., Piani G., 1998]. The drive moment M_E created by the engine is passed to the reel by a system of gears. The value of the moment M_E is determined in the control system presented in Fig. 10.34.

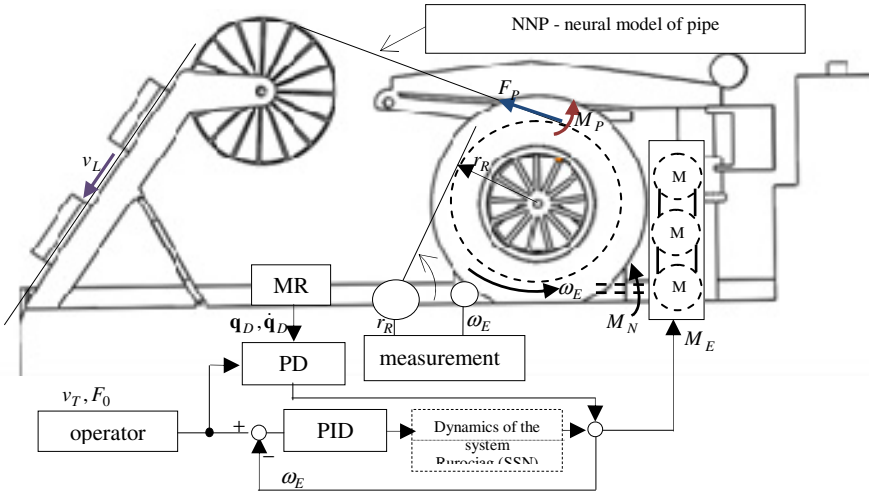

Fig. 10.34. Reel's drive control system

In the computer model, a drive system is represented by a differential equation describing the motion of the reel with pipeline wound onto it and a block performing the calculations of forces and moments caused by the action of the pipeline on the reel (denoted as F_P, M_P). In the concerned application, the operation of this block is based on a model using an artificial neural network. One of the advantages of this approach is short computation time due to the fact that the programme executes only simple operations of multiplication of matrices (containing weight coefficients of the trained network) whose dimensions depend on the numbers of layers and neurons [Osowski S., 1996], [Żurada J., et al., 1996]. To collect data necessary to train the network, a series of simulations was

performed in which the equations (9.95) were integrated for different parameters describing waves. The obtained results were saved as a data set. It is worth to note that the training data was obtained for a model taking into account nonlinear material and geometric models. Details of the mathematical model, architecture of the neural network used, the process of generating training data and its application to determining forces and moments exerted by a pipeline being unwound from a reel are presented in [Szczotka M., 2010].

Practical realization of the proposed control system requires, in addition to replacing the drive with an electric one, measuring the winding diameter r_R of the pipe, the reel's velocity ω_E and the vessel's motion (components of the vector $\mathbf{q}_D$ and its derivative). Control is performed in a feedback loop with a PID controller. The system features also an additional PID controller which introduces an adjustment to the previous PID's response. The additional PID controller enables quick reaction of the system to changes input by the operator and excitation caused by waves. It is an example of a feedforward system which in many cases improves stability and accuracy [Olsson G., Piani G., 1998].

As mentioned, further calculations assume an equivalent model of a pipeline implemented with an artificial neural network. To verify the correctness of obtained results, a comparison is made in Fig. 10.35 between simulations using the full model (a pipeline discretized with the RFE method, discussed in chapter 9.3) ant the functional one. On the graphs, the following denotations are present: SSN – results yielded by an artificial neural network, SES – a pipeline discretized with the RFE method. Computation time for a motion lasting 50 s equalled 5 s approximately, whereas calculations according to the full RFE model with the number of RFEs being 100 take roughly 15 min.

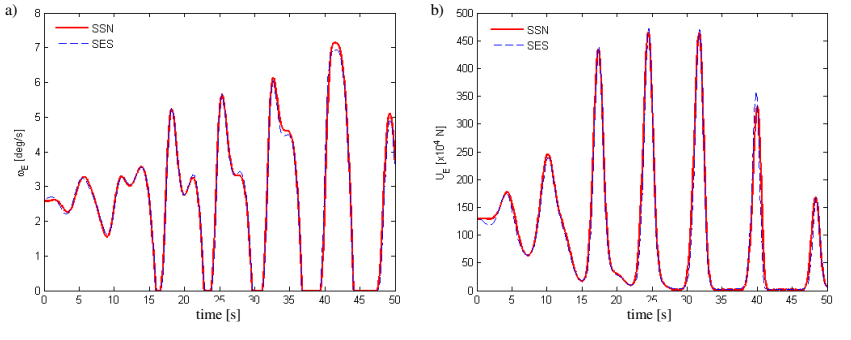

Fig. 10.35. Results of simulation in a passive system: a) reel's velocity, b) tension

10.4.2 Installation of a Pipeline Using the Reel Method with Active Drive System

Sample results of calculations for devices with passive and active reel's drive system are shown in Fig. 10.36. Harmonic excitation of the swaying angle with amplitude $A_\psi = 4^\circ$ and period $T = 8$ s was assumed. Due to structural limitations,

the proposed system cannot fully compensate for the influence of dynamic forces caused by waves in cases when occurring forces exceed some limit values. This shows as variations visible on the graphs of force and angular velocity of the reel.

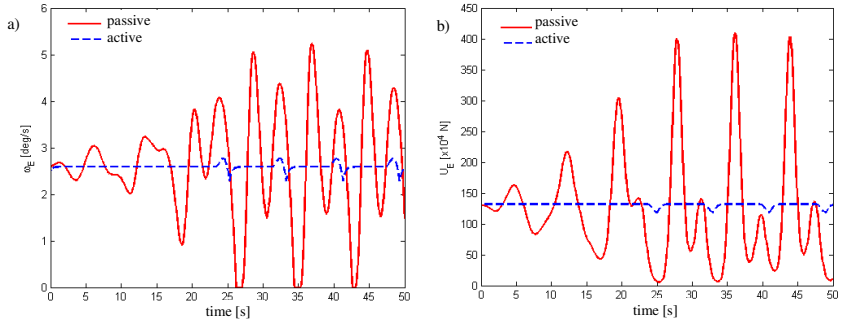

Fig. 10.36. Comparison for passive and active reel drive: a) angular velocity of the reel, b) axial force in the pipeline

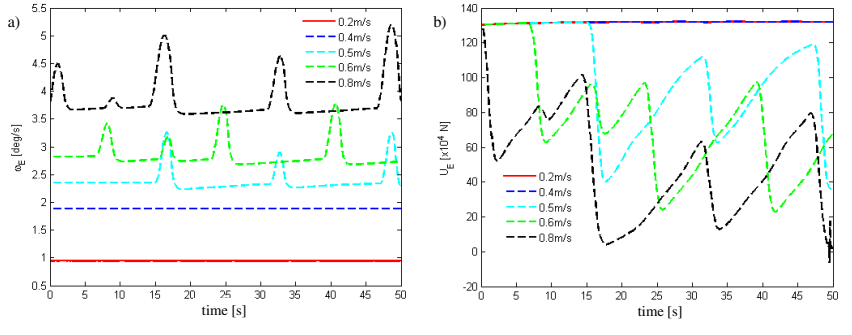

Fig. 10.37. Influence of the speed of laying the pipeline on the behaviour of the system with active compensation for waves: a) reel's velocity, b) tension

One of the limitations not to be forgotten is the available power which can be used to compensate for waves. In the system, successive reduction of drive force after exceeding admissible forces is used. This causes an increase in the reel's velocity (due to forces of inertia caused by the vessel's motion), and further decrease in the moment caused by limited power. The system is capable of returning to the nominal conditions (tension in the pipeline and velocity of the reel) if the operator decreases the tension or waves weakens. Sample results for different settings of the velocity of unwinding the pipeline are summarized by Fig. 10.37.

Note that the assumed power of the drive system (670 kW) is sufficient to operate with constant tension of about 1300 kN when the amplitude $A_\psi = 4^o$, that is under intense wave action. For the vessel's operator also calculating the range of safe, stable operation under variable waves conditions may be of interest.

The parameters of the device's operation (peak changes of the reel's velocity and the axial force in the pipeline) in the selected range of swaying amplitudes from 1° to 4° for periods of waves in the interval between 6 s and 12 s are shown in Fig. 10.38. The values of increment of the angular velocity $\Delta\omega_E$ are given as follows:

$$\Delta\omega_E = \frac{\omega_E^{(\max)} - \omega_E^{(\min)}}{\omega_E^{(0)}} 100\% , \tag{10.73}$$

where $\omega_E^{(\max)}, \omega_E^{(\min)}$ – maximal and minimal velocity of the reel,
$\omega_E^{(0)}$ – nominal velocity of the reel.

Change in the axial force ΔU_E (Fig. 10.88 c and d) is expressed by:

$$\Delta U_E = \max\left\{\left|U_E^{(0)} - \max\left(U_E\right)\right|, \left|U_E^{(0)} - \min\left(U_E\right)\right|\right\}, \tag{10.74}$$

where $U_E^{(0)}$ – axial force at the moment $t = 0$ (nominal value),
$U_E = U_E(t)$ – current value of the force.

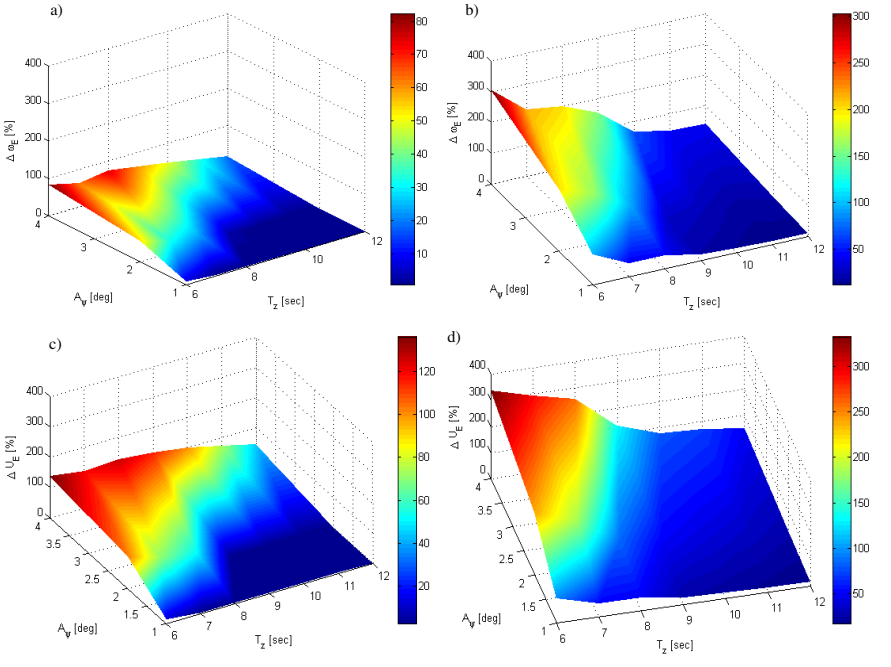

Fig. 10.38. Surfaces describing changes of dynamic parameters with passive and active reel drives a) percentage increments of the reel's velocity in an active system, b) percentage increments of the reel's velocity in a passive system, c) percentage increments of the tension in an active system, d) percentage increments of the tension in an passive system

As the presented graphs indicate, using a system for compensation of waves makes it possible to achieve reduction by a factor greater than three of the dynamic forces and limitation of oscillations of the reel's angular velocity a few times. The graphs were produced for one fixed speed of laying the pipeline equal to 2000 m/h and assumed limits (maximum force passed by the structure of the drive system being 2000 kN and available power 670 kW). The practical effect of employing such a system would be significantly increased efficiency (speed of laying the pipeline) which is a considerable improvement.

The analyses presented are only examples of possible applications of the developed models, algorithms and programmes. It seems particularly useful to employ the model of a drive with automatic adjustment of the force applying tension to the pipeline which allows one to entirely eliminate large overloads in the system with sufficient power. Measuring the vessel's motion is fairly simple. It requires a sensor (e.g. Konsberg Seatex's MRU) to be installed and the reel's angular velocity and winding diameter to be measured. Short computation time, especially when the programme is based on a neural network, is a significant advantage.